

1 **Manuscript #: acp-2015-1022**

2
3 **Title: Impact of Siberia forest fires on the atmospheric environment over the**
4 **Korean Peninsula during summer 2014**

5
6
7 Authors: Jinsang Jung et al.

8
9 **Responses to the reviewer's specific comments and questions:**

10
11 **Reviewer #1 (Comments):**

12
13 **General comments:**

14
15 This manuscript classifies two haze episodes in Korean Peninsula based on different sources,
16 one is from the Siberia forest fire during the late July, 2014, and the other one is from urban and
17 industrial complexes in the East China during the mid July. It also characterizes the chemical
18 compositions of the pollutants during these two haze episodes. This manuscript is well
19 organized, however the presentation of the results part should be improved. You should describe
20 the figure first before you use the information of the figure to support your conclusion.

21
22 **Specific comments:**

23 *I have some concerns about the scatter plots in Figure 11. First, I don't know what black circles*
24 *represent for. I couldn't find description of the black circles anywhere.*

25 **Response:** Following sentence has been added in the caption of Fig. 11 in the revised MS.

26 *“Open black circles represent the remaining sampling days in July 2014.”*

27
28 *Second, the authors mentioned “positive correlation”, “poor correlation”, or “good*
29 *correlation” many times, however, it is not convincing to find correlation from only two or*
30 *three samples. Here, more samples are needed to draw the conclusion on the correlation. Thus,*
31 *this analysis is not a good support to his conclusion.*

32 **Response:** We agreed to the reviewer' comment. We decided to remove the terms “**positive**
33 **correlation**”, “**poor correlation**”, or “**good correlation**” in the revised MS. Specific changes can
34 be seen in the late part of this revision document.

35
36 *Third, if you want to show the trends between different chemical compositions, the scatter plot*
37 *is still not a good tool. Without the time and location of each sample, and so few samples, how*
38 *could you know the trend is increasing or decreasing with time?*

39 **Response:** We agreed to the reviewer' comment. We decided to remove the terms “**positive**
40 **correlation**”, “**poor correlation**”, or “**good correlation**” in the revised MS.

41
42 *This manuscript actually covers two haze episodes in every analysis and show chemical*
43 *composition impacts in both haze episodes. Why does the title only include the part of Siberia*
44 *forest fires?*

45 **Response:** Thank you for the comment. Long-range transport of the Siberia forest fire to the
46 Korean Peninsula rarely happen throughout season. However, long-range transport of the
47 Chinese haze are frequently observed and studied. Thus, we want to focus more on the impact
48 of the Siberia forest fire in the title of the manuscript.

49
50 *Line 57. Define PM10.*

51 **Response:** The phrase “(particulate matter with a diameter of $\leq 10 \mu\text{m}$)” has been added in line
52 56 in the revised MS.

53

54 *Line 96. You have to mention that the anthropogenic pollution episode is not in the same period*
55 *as smoke plumes pollution episode.*

56 **Response:** The phrase “in the middle of July 2014” has been added in lines 96-97 in the revised
57 MS.

58

59 *Section 2. There are a lot of observations from different sites, and those observations are used*
60 *in different analyses of this study. I couldn't remember where they come from when I read the*
61 *later results. I suggest making a table to describe the observation data, include information like*
62 *where do they come from, site numbers, collecting method, sample frequency, used in which*
63 *analysis or which figure, etc.*

64 **Response:** Thank you for the suggestion. We decided to add a table containing summary of
65 measurement parameters and conditions. Following sentence has been added in line 102 in the
66 revised MS.

67 “Table 1 summaries the measurement parameters and conditions of this study.”

68 Following table has been added in table 1 in the revised MS.

69

Table 1. Measurement parameters and conditions of this study.

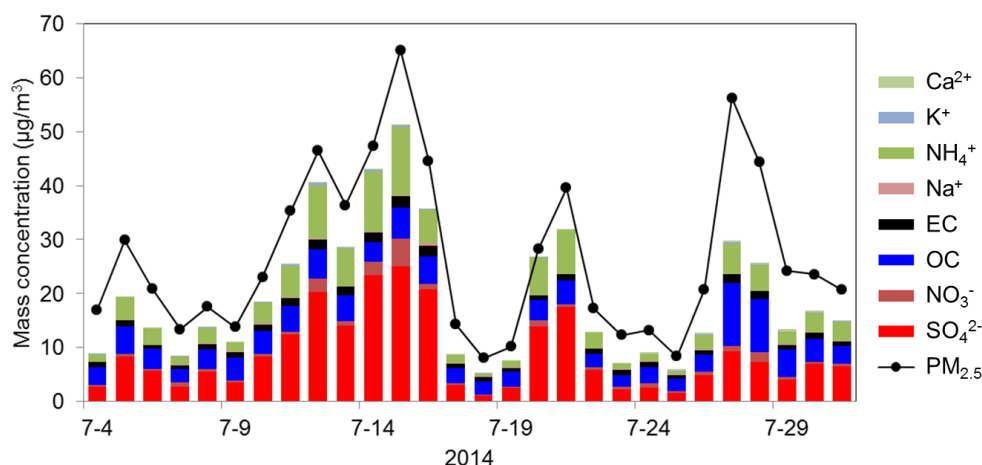
Measurement parameters	Site	Sampling method	Measurement method	Data frequency
PM _{2.5} mass	Daejeon, Korea	Online measurement	Beta-attenuation monitor	1 h
Levoglucosan, Mannosan	Daejeon, Korea	PM _{2.5} filter sampling	High-performance anion-exchange chromatography	1 day
Water-soluble ions (NO ₃ ⁻ , SO ₄ ²⁻ , etc)	Daejeon, Korea	PM _{2.5} filter sampling	Ion Chromatography	1 day
Organic carbon (OC), elemental carbon (EC)	Daejeon, Korea	Online measurement	Semi-continuous OC/EC analyzer	1 h
Aerosol optical depth (AOD)	Yakutsk and Ussuriysk, Russia	Online measurement	Sunphotometer	~15 min

70

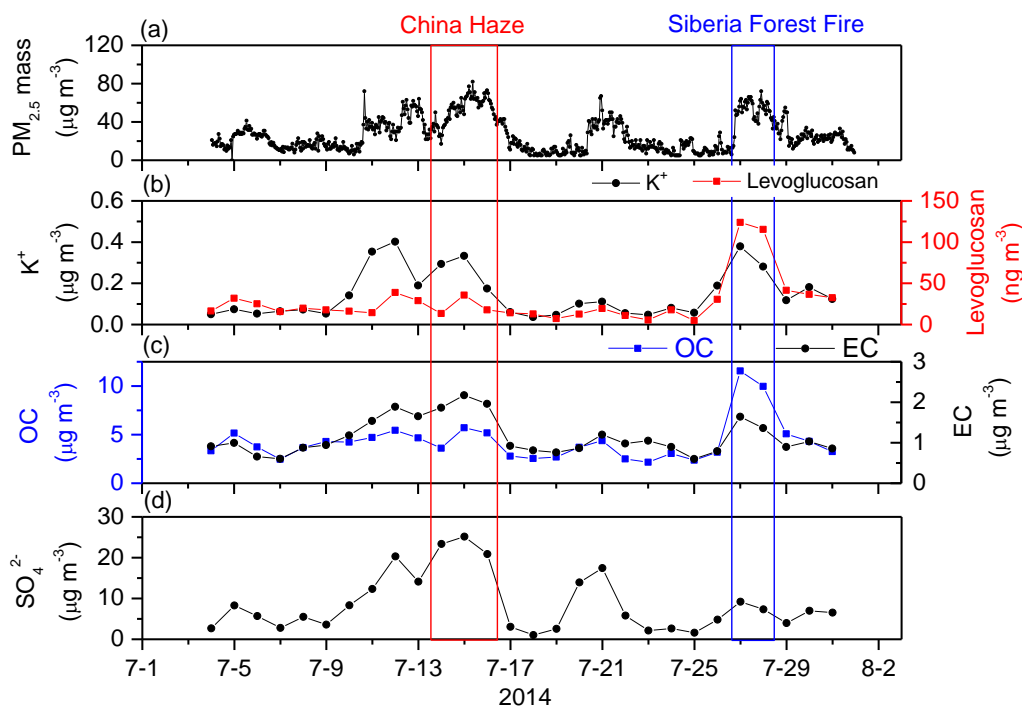
71 *Line 202. The authors only mention two peaks and ignore the peak on 2 July. If you don't want*
72 *readers to focus on the first peak, you can show the period from 8 July to 31 July. At the*
73 *beginning of the results section, it is weird to only mention the point that authors want to focus*
74 *on without explanation of the whole picture. You also need a leading sentence at the beginning*
75 *of section 3 or at the end of section 3.1 to inform that you will focus on the “first” and “second”*
76 *episodes and you are going to show this and that, since you have a very long result section.*

77 **Response:** Thank you for the comment. As reviewer suggested, we have decided to show data
78 from 4 July to 31 July not to confuse readers. The study period of figure 2 and figure 9 were
79 modified as 4 July to 31 July. Please see the modified figure 2 and figure 9 in the revised MS.

80



81
82 Fig. 2. Temporal variations in the chemical components of fine particulate matter (PM_{2.5})
83 at the Daejeon site during July 2014.
84



85
86 Fig. 9. Temporal variations in PM_{2.5} mass, K⁺, levoglucosan, OC, EC, and SO₄²⁻
87 concentrations at the Daejeon site over the entire measurement period.
88

89 *Line 220-222. Where did you initialize the HYSPLIT backward trajectories? Did you randomly*
90 *choose one location in Korean Peninsula or a site location? This information is not mentioned*
91 *here or in section 2. It is the same issue for Fig 7. The trajectories may pass some parts of the*
92 *forest, but it is not obviously to see the trajectories pass the red dots from Fig 3a. Maybe there*
93 *are some red dots covered by the cloud that I couldn't see. The map is not very clear.*

94 **Response:** Following phrase has been added in lines 176-177 in the revised MS.

95 “at the sampling site (36.19 °N, 127.24 °E) in Daejeon, Korea”

96 As we already mentioned in lines 180-183, the HYSPLIT backward trajectory can be used to
97 track general airflow pattern rather than the exact pathway of air masses. As shown in figure 3,

98 we can clearly see similar movement of the Siberia smoke plume from MODIS RGB image in
99 figure 3a compared to the HYSPLIT backward trajectories in figure 3b.

100
101 *Line 234. AOD has dropped to less than 0.5 at late 25 July (Fig 5), and then it increases again.*
102 *Can you explain this?*

103 **Response:** Following sentences have been added in lines 234-238 in the revised MS.

104 “The AOD dropped to <0.5 during 6:00–10:00 UTC, 25 July and increased again during 26 July.
105 Because high AOD at the Yakutsk site was caused by transport of the Siberian smoke plume
106 (Fig. 3), the sharp drop in AOD observed during 25 July can be explained by a change in wind
107 direction at the Yakutsk site.”

108
109 *Line 237-239. The authors demonstrate that the smoke plumes from Siberia fire would impact*
110 *Korean peninsula on 27 July and 28 July in the whole manuscript. However, here the authors*
111 *said the results implied one-day transport. I’m not sure which one is the real conclusion.*

112 **Response:** We agreed to the reviewer’ comment. Sentence in lines 244-245 in the original MS
113 has been modified as follows.

114 “These results again suggest the transport of Siberian smoke plumes to the northern Korean
115 Peninsula.”

116
117 *Line 237-239. Moreover, the author concluded that the sharp increase in Ussuriysk site in 24*
118 *July was due to the Siberia forest fire without showing any evidence. Is it possible that this*
119 *sharp increase is due to other sources?*

120 **Response:** Following sentence has been added in lines 242-243 in the revised MS.

121 “Spatial distributions of AOD from the MODIS satellite data (Fig. 4) clearly show that the
122 Siberian smoke plumes extended over the Ussuriysk site during 24 July 2014.”

123
124 *Line 240-249. Poor description. First, describe left column, and then describe right column.*
125 *Does the right column only represent the Total Attenuated Backscatter along the yellow lines?*
126 *How did the authors define the paths of yellow lines? All these information should be included*
127 *in the description.*

128 **Response:** A paragraph in lines 246-258 in the original MS has been revised as follows.

129 “Figure 6 shows MODIS RGB images and vertical distributions of total attenuated backscatter
130 at a wavelength of 532 nm measured by the CALIPSO satellite during 24, 25, and 27 July 2014.
131 The left column in Fig. 6 shows MODIS RGB images taken during the Siberian smoke episode.
132 These images show smoke plumes originating from the Siberian forest and being transported
133 over northeastern China. The yellow lines over the images in the left column of Fig. 6 indicate
134 the route of the CALIPSO satellite, and correspond to the x-axis of the backscatter plots shown
135 in the right column of Fig. 6. In the total attenuated backscatter measurement plots (Fig. 6,
136 right), red and yellow represent atmospheric aerosol particles and white represents clouds.
137 Figure 6a and b clearly show that between 24 and 25 July 2014, a smoke layer existed
138 approximately 3–5 km in height near the source region of the Siberian forest fires. As shown in
139 Fig. 6c, the height of the smoke layer decreased to below 2 km on 27 July 2014 as it reached the
140 Korean Peninsula.”

141
142 *Line 329-335. Are there only 3 points for Chinese haze episode and 2 points for Siberia forest*
143 *fire episode? There are too few samples to get any meaningful correlation.*

144 **Response:** We agreed with the reviewer’ comment. Following sentence was deleted.

145 “Positive correlation was obtained between levoglucosan and OC concentrations during the
146 Siberia forest fire and Chinese haze episodes in Fig. 11a.”

147 Lines in 329-333 in the original MS have been modified as follows. Please see lines 352-357 in
148 the revised MS.

149 “OC concentrations increased as levoglucosan and K⁺ concentrations increased during the
 150 Siberian forest fire episode (Fig. 11a). Elevated OC/EC ratios were also observed during the
 151 Siberian forest fire episode (7.18 ± 0.2). Simultaneous increases in K⁺, OC (Fig. 11b), and
 152 levoglucosan concentrations (Fig. 11c) during the Siberian forest fire episode suggest that the
 153 K⁺ originated primarily from the smoke plume during the Siberian forest fire episode.”

154
 155 *Line 336. “Good correlations”. Add the values of the correlations. Please be quantitative.*

156 *Line 338. “different correlation patterns”. I didn’t see obvious difference from the figure. Could
 157 you describe more clearly about the patterns’ difference?*

158 **Response:** Thank you for the comment. After considering reviewer’s comments in lines 336
 159 and 338, the sentences starting “Good correlations of K⁺ ...” in lines 336-340 have been revised
 160 as follows. Please see lines 358-364 in the revised MS.

161 “OC and levoglucosan concentrations observed during the Chinese haze episode are similar to
 162 those observed during the non-episode period, as shown in Fig. 11a. However, small increases
 163 in K⁺ concentration were observed during the Chinese haze episode, as shown in Fig. 11b,
 164 resulting in relatively small levoglucosan/K⁺ ratios during the Chinese haze episode ($0.08 \pm$
 165 0.03) compared with those during the Siberian forest fire episode (0.37 ± 0.06). This difference
 166 in levoglucosan/K⁺ ratios can be explained as follows.”

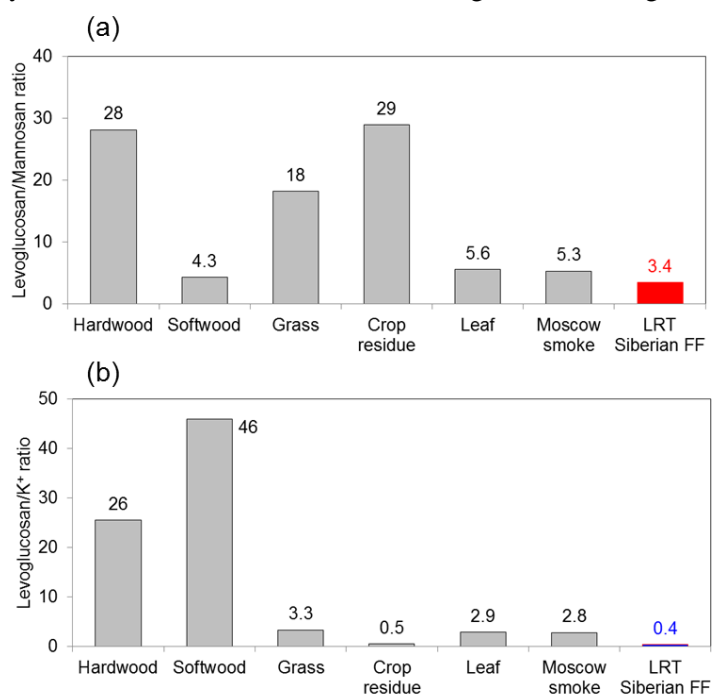
167
 168 *Line 349. “Poor correlations”. Please be quantitative.*

169 **Response:** The phrase “Poor correlations of K⁺ with OC and levoglucosan concentrations
 170 during the Chinese haze episode suggest” in lines 373-375 in the original MS has been modified
 171 as follows.

172 “The lack of significant increases in OC/EC ratio (2.4 ± 0.4), and OC and levoglucosan
 173 concentrations during the Chinese haze episode compared with non-episode measurements
 174 suggests”

175
 176 *Figure 12. I suggest changing the color of the last bar in order to distinguish this study from
 177 other referenced studies.*

178 **Response:** Thank you for the comment. The last bar of Fig. 12 was changed as follows.



179
 180

181
182

183 **Reviewer #2 (Comments):**

184
185
186 **General Comments:**

187
188 Dear Authors, Thank you for this manuscript. It describes an interesting case study of long-
189 range transport of Siberian smoke to Korea. I think this paper will produce an interesting
190 contribution to ACP.

191 My main question regarding your analysis is that you do not discuss the potential contribution
192 of biofuel to the southern China haze event. Many literature sources indicate that biofuel is a
193 significant contributor to the energy mix and to the air pollution in rural Chinese areas. I think
194 your analysis would be strengthened if you examined the chemical composition of the southern
195 Chinese haze in the context of literature estimates of biofuel consumption in the southern
196 Chinese region. The recent paper by Rongrong Wu et al. (doi:10.1016/j.atmosenv.2015.12.015)
197 would be a good place to start.

198 **Response:** Thank you for the comment. Following paragraph has been added in lines 298-314
199 in the revised MS.

200 “It has been reported that biomass burning (including biofuel) contributed 14.1% of the total
201 VOC emissions in China during 2012, whereas in Anhui province the contribution of biomass
202 combustion to VOC emissions was 28.7% (Wu et al., 2016). Li et al. (2015) reported that
203 biomass burning contributed 58% of OC in Nanjing, China during summer 2012, suggesting
204 that biomass burning is the dominant source of OC in this region. Du et al. (2011) classified the
205 haze events in Shanghai, China during summer 2009 into three categories: biomass-burning
206 induced (high K^+ , low SO_4^{2-} and NO_3^-), complicated (high SO_4^{2-} and NO_3^- , good correlation
207 between K^+ and SO_4^{2-} and NO_3^-), and secondary (high SO_4^{2-} and NO_3^- , low K^+) pollution.
208 Because Anhui, Nanjing, and Shanghai are located near the source of the long-range transported
209 Chinese haze (Fig. 8), the chemical composition of pollution in those areas can be used to
210 understand the Chinese haze episode observed in this study. Temporal patterns in K^+
211 concentration are similar to those of SO_4^{2-} , and a sharp increase in SO_4^{2-} concentration was
212 observed during the Chinese haze episode (Fig. 9). This type of pollution episode is similar to
213 the ‘complicated’ pollution described by Du et al. (2011), and suggests that the Chinese haze
214 episode was caused mainly by secondary aerosol such as SO_4^{2-} and NH_4^+ , rather than by
215 biomass burning emissions.”

216
217 Three references were added in the reference section.

218 Du, H., Kong, L., Cheng, T., Chen, J., Du, J., Li, L., Xia, X., Leng, C., and Huang, G.: Insights
219 into summertime haze pollution events over Shanghai based on online water-soluble ionic
220 composition of aerosols, *Atmos. Environ.*, 45, 5131–5137, 2011.

221 Li, B., Zhang, J., Zhao, Y., Yuan, S., Zhao, Q., Shen, G., and Wu, H.: Seasonal variation of
222 urban carbonaceous aerosols in a typical city Nanjing in Yangtze River Delta, China, *Atmos.*
223 *Environ.*, 106, 223–231, 2015.

224 Wu, R., Bo, Y., Li, J., Li, L., Li, Y., and Xie, S.: Method to establish the emission inventory of
225 anthropogenic volatile organic compounds in China and its application in the period 2008-2012,
226 *Atmos. Environ.*, 127, 244–254, 2016.

227
228 Apart from that, this paper is scientifically sound and the conclusions are reasonable. I believe
229 this paper would benefit from a thorough editing to improve grammar and remove typographical
230 errors. Best of luck with your revisions, and thank you again.

231 **Response:** Thank you for the comment. The revised MS has been proofread by a English native
232 speaker.

234
235 Impact of Siberian forest fires on the atmosphere over the Korean
236 Peninsula during summer 2014

237

238 Jinsang Jung^{a,*}, Youngsook Lyu^b, Minhee Lee^b, Taekyung Hwang^b, Sangil Lee^a,
239 Sanghyub Oh^a

240

241 ^aCenter for Gas Analysis, Korea Research Institute of Standards and Science (KRISS),
242 Daejeon 34113, Republic of Korea

243 ^bDepartment of Climate and Air Quality Research, National Institute of Environmental
244 Research, Daejeon 34944, Republic of Korea

245

246

247 Running title: Russian Forest Fire

248

249 Last modified: May 06, 2016

250 To be submitted to *Atmospheric Chemistry and Physics*

251

252 *Corresponding author: Jinsang Jung (jsjung@kriss.re.kr)

253

254 **Abstract**

255 Extensive forest fires occurred during late July 2014 across the forested region of
256 Siberia, Russia. Smoke plumes emitted from Siberian forest fires underwent long-range
257 transport over Mongolia and northeast China to the Korean Peninsula, which is located
258 ~3000 km south of the Siberian forest. A notably high aerosol optical depth of ~4 was
259 observed at a wavelength of 500 nm near the source of the Siberian forest fires. Smoke
260 plumes reached 3–5 km in height near the source and fell below 2 km over the Korean
261 Peninsula. Elevated concentrations of levoglucosan were observed ($119.7 \pm 6.0 \text{ ng m}^{-3}$),
262 which were ~4.5 times higher than those observed during non-event periods in July
263 2014. During the middle of July 2014, a haze episode occurred that was primarily
264 caused by the long-range transport of emission plumes originating from urban and
265 industrial complexes in East China. Sharp increases in SO_4^{2-} concentrations (to $23.1 \pm$
266 $2.1 \mu\text{g m}^{-3}$) were observed during this episode. The haze caused by the long-range
267 transport of Siberian forest fire emissions was clearly identified by relatively high
268 organic carbon (OC)/elemental carbon (EC) ratios (7.18 ± 0.2) and OC/ SO_4^{2-} ratios
269 (1.31 ± 0.07) compared with those of the Chinese haze episode (OC/EC ratio: 2.4 ± 0.4 ;
270 OC/ SO_4^{2-} ratio: 0.21 ± 0.05). Remote measurement techniques and chemical analyses of
271 the haze plumes clearly show that the haze episode that occurred during late July 2014
272 was caused mainly by the long-range transport of smoke plumes emitted from Siberian
273 forest fires.

274

275 1. Introduction

276 Forest fires emit large amounts of gaseous and particulate pollutants into the
277 atmosphere, including carbon dioxide (CO₂), carbon monoxide (CO), methane (CH₄),
278 nitrogen oxides (NO_x), ammonia (NH₃), particulate matter (PM), non-methane
279 hydrocarbon (NMHC), and other chemical species (Crutzen and Andreae, 1990). These
280 pollutants alter the regional climate of downwind areas by altering ambient temperature,
281 cloud properties, and precipitation efficiency (Jeong et al., 2008; Youn et al., 2011;
282 Jeong et al., 2014). They also influence the air quality of downwind areas in urban,
283 ocean, and Arctic regions through long-range atmospheric transport (Carvalho et al.,
284 2011; Quennehe et al., 2012; Schreier et al., 2015).

285 During a severe forest fire episode in Moscow, Russia in August 2010, notably high
286 concentrations of total carbon (mean of 202 µg m⁻³) and levoglucosan (3.1 µg m⁻³)
287 were observed with an elevated organic carbon/elemental carbon (OC/EC) ratio of 27.4
288 (Popovicheva et al., 2014). Total carbon concentrations exceeded 10 times that during
289 non-event periods in Moscow (Popovicheva et al., 2014). During severe forest fires in
290 Siberia in May 2003, the surface PM₁₀ (particulate matter with a diameter of ≤10 µm)
291 and O₃ concentrations in downwind areas increased by 5–30 µg m⁻³ and 3–20 ppbv,
292 respectively, and this had important implications for air quality over East Asia (Jeong et
293 al., 2008).

294 Russia is covered by over 800 million hectares of forest, which is equal to 50 billion
295 tons of growing carbon stock, where annually about 1% is damaged by fires (Bondur,
296 2010; Popovicheva et al., 2014). Russian boreal forests are subjected to frequent
297 wildfires. Each year, 10,000–35,000 forest fires covering 5000–53,000 km² (including
298 4000–10,000 km² of high intensity, stand-replacing fires) are detected in actively

299 protected portions of Russian forests (Bartalev et al., 1977; Isaev et al., 2002; Mei et al.,
300 2011). Approximately 12,000–34,000 wildfires occurred every year between 1974 and
301 1993 (Conard and Eduard, 1996), which makes Siberia a major boreal forest fire area in
302 global terms.

303 Frequent forest fires over Siberia have an impact on downwind areas in Mongolia,
304 China, Korea, and the Northwest Pacific through long-range atmospheric transport
305 (Kajii et al., 2002; Kanaya et al., 2003; Lee et al., 2005; Jeong et al., 2008; Youn et al.,
306 2011). In May 2003, intense forest fires occurred over Siberia (Lee et al., 2005; Jeong et
307 al., 2008; Youn et al., 2011). Satellite observations clearly show the transport of smoke
308 plumes emitted from Siberian forest fires through Mongolia and eastern China, south to
309 the Korean Peninsula (Lee et al., 2005). Simulations by Youn et al. (2011) showed a
310 significant surface cooling of -3.5 K over forested regions of Siberia. These simulations
311 also showed that smoke aerosol affected large-scale circulation and resulted in an
312 increase in average rainfall rates of 2.9 mm day⁻¹ over the Northwest Pacific. Jeong et al.
313 (2008) reported that smoke plumes from Siberian forest fires in May 2003 acted mainly
314 as a cooling agent, resulting in a negative radiative forcing of -5.8 W m⁻² at the surface
315 over East Asia.

316 Severe wildfires occurred in the forested regions of Russia during summer 2014.
317 The intensity of wildfires during this period was three times larger than in 2013.
318 According to Russia's ITAR-TASS news agency, ~12,600 forest fires had burned over
319 1.8 million hectares as of 16 July 2014. During this time, the most forest fires occurred
320 in the Irkutsk and Yakutsk areas of Siberia. Over 200 forest fires covering 92,000
321 hectares occurred in Siberian forested regions as of 16 July 2014
322 (<http://tass.ru/en/russia/740878>). MODIS satellite RGB images clearly show that these

323 smoke plumes lasted more than a week and were transported south to Mongolia,
324 northern China, and the Korean Peninsula.

325 In this study, we investigate the smoke plumes emitted from Siberian forest fires
326 during late July 2014 and their long-range atmospheric transport to the Korean
327 Peninsula. The transport mechanism of these plumes is investigated based on satellite
328 image analysis and satellite-based lidar observations. We also characterize the chemical
329 composition of these plumes over the Korean Peninsula. Chemical characteristics of
330 anthropogenic pollutants from East China transported to the Korean Peninsula **in the**
331 **middle of July 2014** are also investigated and compared with those originating from
332 Siberian forest fires.

333

334 2. Experimental Methods

335 2.1 Atmospheric aerosol sampling and sample preparation

336 **Table 1 summarizes the measurement parameters and conditions of this study.** Daily
337 PM_{2.5} (particulate matter with a diameter of $\leq 2.5 \mu\text{m}$) sampling was carried out at a
338 regional air-quality monitoring station (36.19°N, 127.24°E) centrally located in Daejeon,
339 Korea, from **4** to 31 July 2014. The samples were collected on pre-baked quartz fiber
340 filters (47 mm diameter, Pall-Life Sciences, USA) using an aerosol sampler (PMS-103,
341 APM, Korea) at a flow rate of 16.7 L min^{-1} on the rooftop of a comprehensive
342 monitoring building (~15 m above the ground) of the National Institute of
343 Environmental Research in Korea. Before and after sampling, the filter samples were
344 wrapped with aluminum foil and stored in a freezer at $-20 \text{ }^\circ\text{C}$. A total of 31 filter
345 samples were collected in this study, and additional field blank filters were collected
346 before and after the sampling period.

347 Ultrapure water used in this study was prepared using a Labpure S1 filter and an
348 ultra-violet (UV) lamp (ELGA, PureLab Ultra, USA). Resistivity and total organic
349 carbon (TOC) values of the ultrapure water were maintained at $18.2 \text{ M}\Omega \text{ cm}^{-1}$ and 4 ppb,
350 respectively. To measure carbohydrates and water-soluble ions, a quarter of each filter
351 sample was extracted with 10 mL of ultrapure water under ultrasonication for 30 min,
352 and then passed through a disk filter (0.45 mm, Millipore, Millex-GV, Germany). Water
353 extracts were stored in a refrigerator at 4 °C before analysis.

354

355 2.2 Analysis of the chemical composition of fine particles

356 Mass concentrations of $\text{PM}_{2.5}$ were measured using a beta-attenuation technique
357 (BAM 1020, Met One Instruments), with an hourly averaging time resolution. The
358 manufacturer reported the detection limit and measurement error of the beta-attenuation
359 technique as $3.6 \mu\text{g m}^{-3}$ and 8%, respectively. In addition to $\text{PM}_{2.5}$ mass concentrations,
360 the daily-averaged chemical composition of $\text{PM}_{2.5}$ was characterized through filter
361 sampling and laboratory analysis. Because the $\text{PM}_{2.5}$ chemical composition
362 measurements were made on a daily basis, daily-averaged $\text{PM}_{2.5}$ mass and chemical
363 compositions were used in this study.

364

365 2.2.1 Levoglucosan and mannosan analysis

366 Levoglucosan and mannosan were analyzed using an improved high-performance
367 anion-exchange chromatography (HPAEC) method with pulsed amperometric detection
368 (PAD) (Engling et al., 2006; Jung et al., 2014). The HPAEC-PAD system uses an ion
369 chromatograph consisting of an electrochemical detector and gold electrode unit, along
370 with an AS40 auto-sampler (Dionex ICS-15000, Thermo Fisher Scientific, USA).

371 Levoglucosan and mannosan were separated in a CarboPak MA1 analytical column (4 ×
372 250 mm) using a sodium hydroxide solution as the eluent. The detection limits of
373 levoglucosan and mannosan were 3.0 and 0.7 ng m⁻³, respectively. The calculated
374 values for analytical error, defined as the ratio of the standard deviation to the average
375 value, obtained from triplicate analyses of filter samples, were 1.9% and 0.73% for
376 levoglucosan and mannosan, respectively.

377

378 2.2.2 Water-soluble inorganic ion analysis

379 Water-soluble inorganic ions were analyzed using an ion chromatograph (Dionex
380 ICS-15000, Thermo Fisher Scientific, USA). Nitrate (NO₃⁻) and sulfate (SO₄²⁻) were
381 separated using an IonPAC AS15 column with a 20 mM potassium hydroxide (KOH)
382 eluent at a flow rate of 0.5 mL min⁻¹. The detection limits of NO₃⁻ and SO₄²⁻, which are
383 defined as three times the standard deviation of field blanks, were 0.01 and 0.11 µg m⁻³,
384 respectively. The analytical errors associated with NO₃⁻ and SO₄²⁻ were 2.3% and 1.7%,
385 respectively. Sodium (Na⁺), ammonium (NH₄⁺), potassium (K⁺), calcium (Ca²⁺), and
386 magnesium (Mg²⁺) were separated using an IonPac CS-12A column (4 × 250 mm) with
387 a 38 mM methanesulfonic acid (MSA) eluent at a flow rate of 1.0 mL min⁻¹. The
388 detection limits of NH₄⁺ and K⁺ were 0.03 and 0.006 µg m⁻³, respectively. The
389 analytical errors associated with NH₄⁺ and K⁺ were 1.4% and 0.73%, respectively.

390

391 2.2.3 Organic carbon/elemental carbon analysis

392 Carbonaceous PM_{2.5} was measured using a semi-continuous organic
393 carbon/elemental carbon (OC/EC) analyzer (Model RT3140, Sunset Lab). The air
394 samples were drawn through a PM_{2.5} sharp-cut cyclone at 8 L min⁻¹. The sampled

395 aerosol was then passed through a multichannel parallel-plate denuder with a carbon-
396 impregnated filter to remove semi-volatile organic vapors, and then collected on a
397 quartz-fiber filter. The sampled aerosol was analyzed based on the thermal-optical
398 transmittance (TOT) protocol for pyrolysis correction and the NIOSH (National
399 Institute for Occupational Safety and Health) method 5040 temperature profile (Birch
400 and Cary, 1996; Jung et al., 2010). External calibration was performed using known
401 amounts of sucrose. The detection limit of both OC and EC is $0.5 \mu\text{g C m}^{-3}$ for a 1 hr
402 time resolution, according to the manufacturer. The uncertainty of OC and EC
403 measurements has been reported as 5% (Polidori et al., 2006).

404

405 2.3 Satellite aerosol optical depth and air mass backward trajectories

406 The NOAA/ARL HYSPLIT (HYbrid Single-Particle Lagrangian Trajectory) air
407 mass backward trajectory analysis (Draxler and Rolph, 2015; Rolph, 2015) and
408 Moderate Resolution Imaging Spectro-radiometer (MODIS) satellite image analysis
409 were used to characterize potential source regions and the transport pathway of the haze
410 plume. Air mass backward trajectories ending at the sampling site (36.19°N, 127.24°E)
411 in Daejeon, Korea were computed for heights of 200, 500, and 1000 m above ground
412 level (AGL) using the HYSPLIT model. All back-trajectories were calculated at 00:00
413 UTC and 12:00 UTC (09:00 LT and 21:00 LT, respectively), extending back 96 h with
414 a 1 h time interval. The calculated air mass pathways indicate the general airflow
415 pattern rather than the exact pathway of air masses, because the typical error in traveled
416 distance is up to 20% for trajectories computed from analyzed wind fields (Stohl, 1998).

417 This study used aerosol optical depth (AOD) data retrieved using the NASA
418 MODIS algorithm version V5.2, referred to as Collection 005 (C005) (Levy et al.,

419 2007a, b), which are part of the MODIS Terra/Aqua Level-2 gridded atmospheric data
420 product and are available on the MODIS web site (<http://modis.gsfc.nasa.gov/>). Cloud-
421 screened level 1.5 sun-photometer data at sites in Yakutsk (61.66 °N, 129.37 °E; 118 m
422 above sea level) and Ussuriysk (43.70°N, 132.16°E; 280 m above sea level) in Russia
423 were obtained from the AERONET site (<http://aeronet.gsfc.nasa.gov>). This study used
424 total column-integrated spectral AOD determined using the AERONET algorithm
425 (Dubovik and King, 2000).

426 CALIOP (Cloud-Aerosol Lidar with Orthogonal Polarization) is a space-based lidar
427 system onboard the Cloud Aerosol Lidar and Infrared Pathfinder Satellite Observations
428 (CALIPSO) satellite launched in 2006 (Winker et al., 2009). This study used version
429 2.30 data of total attenuated backscatter at 532 nm. Expedited CALIPSO images were
430 obtained from the CALIPSO website ([http://www-
431 calipso.larc.nasa.gov/products/lidar/browse_images/show_calendar.php](http://www-calipso.larc.nasa.gov/products/lidar/browse_images/show_calendar.php)).

432

433 3. Results and Discussion

434 3.1 Overview of the chemical composition of PM_{2.5}

435 Figure 2 shows temporal variations in the chemical composition of PM_{2.5} at the
436 Daejeon site throughout the entire measurement period. Daily average PM_{2.5} mass
437 concentrations ranged from 8.0 to 65.1 $\mu\text{g m}^{-3}$ with an average of $26.8 \pm 15.4 \mu\text{g m}^{-3}$.
438 Two peaks in PM_{2.5} mass concentration were observed during 12–16 July (first episode)
439 and 27–28 July 2014 (second episode). PM_{2.5} mass concentrations reached 65.1 and
440 56.2 $\mu\text{g m}^{-3}$ during the first and second episodes, respectively. The temporal variations
441 in the sum of PM_{2.5} chemical compositions show a similar pattern to that of total PM_{2.5}
442 mass (Fig. 2). The largest contribution to PM_{2.5} mass during the measurement period

443 came from SO_4^{2-} , which had a mean of $8.8 \pm 7.0 \mu\text{g m}^{-3}$, followed by OC ($4.3 \pm 2.0 \mu\text{g}$
444 m^{-3}), NH_4^+ ($4.3 \pm 3.3 \mu\text{g m}^{-3}$), EC ($1.1 \pm 0.4 \mu\text{g m}^{-3}$), and NO_3^- ($1.0 \pm 1.1 \mu\text{g m}^{-3}$), with
445 minor contributions from Ca^{2+} , K^+ , and Na^+ .

446

447 3.2 Classification of haze episodes during summer 2014

448 3.2.1 Long-range transported smoke plumes from Siberian forest fires

449 The MODIS RGB images clearly show severe smoke plumes over the Siberian
450 forested region during late July 2014. Figure 3a shows a typical example from 25 July
451 2014 of satellite RGB images of the smoke plumes emitted from Siberian forest fires
452 and their atmospheric transport to the south. Fire events over the Siberian forested
453 region are indicated by red dots in Fig. 3a. It is clear that the smoke plumes originated
454 in Siberia and were transported south to the Korean Peninsula across Mongolia and
455 northeast China. HYSPLIT backward trajectory analyses (Fig. 3b) also indicate that
456 the air masses originated in the Siberian forested region and were transported to the
457 Korean Peninsula between 26 and 28 July 2014.

458 Figure 4 shows the horizontal distribution of AOD over East Asia from 23 to 28 July
459 2014. High values of AOD were observed over the Siberian forested region on 23 July,
460 when forest fires occurred. Peak values of AOD were then observed to shift southward
461 to northeast China and the Korean Peninsula from 23 to 28 July 2014 (Fig. 4). These
462 horizontal distributions of AOD also support the transport of smoke plumes emitted
463 from Siberian forest fires onto the Korean Peninsula during late July 2014.

464 Figure 5 shows temporal variations in AOD measured using a sun-photometer at the
465 Yakutsk and Ussuriysk sites. The Yakutsk site is located near the source of Siberian
466 forest fire emissions, whereas the Ussuriysk site is located just to the north of the

467 Korean Peninsula (Fig. 3). The measured AOD at the Yakutsk site started to increase
468 from 23 July, and high AOD continued until 26 July 2014. The AOD dropped to <0.5
469 during 6:00–10:00 UTC, 25 July and increased again during 26 July. Because high
470 AOD at the Yakutsk site was caused by transport of the Siberian smoke plume (Fig. 3),
471 the sharp drop in AOD observed during 25 July can be explained by a change in wind
472 direction at the Yakutsk site. The maximum AOD (~4) was observed at the Yakutsk
473 site on 24 July 2014 during a Siberian forest fire event. High values for AOD were
474 observed for 4 days at the Yakutsk site during the Siberian forest fire episode.
475 Interestingly, a sharp increase in AOD was also observed at the Ussuriysk site on 24
476 July 2014. Spatial distributions of AOD from the MODIS satellite data (Fig. 4) clearly
477 show that the Siberian smoke plumes extended over the Ussuriysk site during 24 July
478 2014. These results again suggest the transport of Siberian smoke plumes to the
479 northern Korean Peninsula.

480 Figure 6 shows MODIS RGB images and vertical distributions of total attenuated
481 backscatter at a wavelength of 532 nm measured by the CALIPSO satellite during 24,
482 25, and 27 July 2014. The left column in Fig. 6 shows MODIS RGB images taken
483 during the Siberian smoke episode. These images show smoke plumes originating from
484 the Siberian forest and being transported over northeastern China. The yellow lines
485 over the images in the left column of Fig. 6 indicate the route of the CALIPSO satellite,
486 and correspond to the x-axis of the backscatter plots shown in the right column of Fig.
487 6. In the total attenuated backscatter measurement plots (Fig. 6, right), red and yellow
488 represent atmospheric aerosol particles and white represents clouds. Figure 6a and b
489 clearly show that between 24 and 25 July 2014, a smoke layer existed approximately
490 3–5 km in height near the source region of the Siberian forest fires. As shown in Fig.

491 6c, the height of the smoke layer decreased to below 2 km on 27 July 2014 as it
492 reached the Korean Peninsula.

493 The spatial distribution of AOD obtained from the MODIS and CALIPSO satellite
494 observations, and the HYSPLIT air mass backward trajectory analysis indicate that
495 smoke plumes originated from Siberian forest fires between 23 and 24 July 2014 and
496 were transported over 3000 km south to the Korean Peninsula between 27 and 28 July
497 2014. Ground-based AOD measurements using a sun-photometer near the Siberian
498 forest fire area and on the Korean Peninsula also support the transport of a smoke
499 plume originating from Siberian forest fires onto the Korean Peninsula. Thus, the
500 smoke episode observed between 27 and 28 July 2014 is hereafter referred to as the
501 Siberian forest fire episode.

502

503 3.2.2 Long-range transported haze from Asian continental outflow

504 Besides the haze episode caused by the long-range transport of smoke emitted from
505 Siberian forest fires during late July 2014, another haze episode was observed at the
506 Daejeon site between 14 and 16 July 2014, as shown in Fig. 2. The MODIS RGB image
507 from 14 July (Fig. 7) shows a severe haze plume originating from East China and
508 extending to the Korean Peninsula across the Yellow Sea. HYSPLIT backward air mass
509 trajectories also indicate the transport of air masses originating in East China to the
510 Korean Peninsula over the Yellow Sea between 15 and 16 July 2014.

511 The region of East China extending from Beijing to Shanghai consists of heavily
512 populated and industrialized cities (Chan and Yao, 2008). Large amounts of
513 anthropogenic pollutants are emitted from this region (Li et al., in press). Figure 8
514 shows the horizontal distribution of MODIS AOD over East Asia from 13 to 16 July

515 2014. A trail of high AOD extending from East China to the Korean Peninsula over the
516 Yellow Sea is evident, which suggests that the haze episode observed between 14 and
517 16 July 2014 was caused primarily by long-range transport of pollutants originating
518 from East China. Thus, the haze episode observed between 14 and 16 July is hereafter
519 referred to as the Chinese haze episode.

520

521 3.3 Chemical characterization of long-range transported haze plumes

522 3.3.1 Comparison of PM_{2.5} chemical composition during haze episodes

523 Figure 9 shows temporal variations in PM_{2.5} mass concentration and selected
524 chemical components. During the Chinese haze episode, elevated concentrations of
525 SO₄²⁻ ($23.1 \pm 2.1 \mu\text{g m}^{-3}$) and K⁺ ($0.27 \pm 0.08 \mu\text{g m}^{-3}$) were observed, whereas
526 elevated concentrations of levoglucosan ($119.6 \pm 6.0 \text{ ng m}^{-3}$), K⁺ ($0.33 \pm 0.07 \mu\text{g m}^{-3}$),
527 and OC ($10.8 \pm 1.1 \mu\text{g m}^{-3}$) were measured during the Siberian forest fire episode. As
528 shown in Fig. 9, OC concentrations were relatively constant throughout the
529 measurement period, except during the Siberian forest fire episode. However, several
530 peaks in SO₄²⁻ concentration were observed, with the highest peak occurring during
531 the Chinese haze episode.

532 It has been reported that biomass burning (including biofuel) contributed 14.1% of
533 the total VOC emissions in China during 2012, whereas in Anhui province the
534 contribution of biomass combustion to VOC emissions was 28.7% (Wu et al., 2016).
535 Li et al. (2015) reported that biomass burning contributed 58% of OC in Nanjing,
536 China during summer 2012, suggesting that biomass burning is the dominant source of
537 OC in this region. Du et al. (2011) classified the haze events in Shanghai, China during
538 summer 2009 into three categories: biomass-burning induced (high K⁺, low SO₄²⁻ and

539 NO_3^-), complicated (high SO_4^{2-} and NO_3^- , good correlation between K^+ and SO_4^{2-} and
540 NO_3^-), and secondary (high SO_4^{2-} and NO_3^- , low K^+) pollution. Because Anhui,
541 Nanjing, and Shanghai are located near the source of the long-range transported
542 Chinese haze (Fig. 8), the chemical composition of pollution in those areas can be used
543 to understand the Chinese haze episode observed in this study. Temporal patterns in K^+
544 concentration are similar to those of SO_4^{2-} , and a sharp increase in SO_4^{2-} concentration
545 was observed during the Chinese haze episode (Fig. 9). This type of pollution episode
546 is similar to the ‘complicated’ pollution described by Du et al. (2011), and suggests
547 that the Chinese haze episode was caused mainly by secondary aerosol such as SO_4^{2-}
548 and NH_4^+ , rather than by biomass burning emissions.

549 Figure 10 shows relative contributions to $\text{PM}_{2.5}$ mass during the Chinese haze and
550 Siberian forest fire episodes. Concentrations of organic aerosol (OM) were
551 reconstructed from measured OC concentrations by multiplying the OM/OC ratio of
552 1.8 that was measured using an aerosol mass spectrometer in Korea from spring to fall
553 2011 in the Asian continental outflow (Prof. T. Lee, pers. comm.). Huang et al. (2011)
554 reported a similar OM/OC ratio of 1.77 ± 0.08 measured at a downwind site of the
555 highly polluted Pearl River Delta cities in China during fall 2008. During the Chinese
556 haze episode, SO_4^{2-} was found to be the dominant species in $\text{PM}_{2.5}$ mass with an
557 average contribution of 44.2%, followed by OM (16.6%) and NH_4^+ (19.1%). This
558 result suggests that the Chinese haze episode can be attributed primarily to
559 anthropogenic pollutants (possibly emissions from industrial complexes and urban
560 cities in East China). However, during the Siberian forest fire episode, OM was the
561 dominant species in $\text{PM}_{2.5}$ mass with an average contribution of 38.6%, followed by
562 SO_4^{2-} (16.5%) and NH_4^+ (10.0%). The high concentration of OM indicates that the

563 Siberian forest fire episode originated primarily from biomass burning.

564

565 3.3.2 Comparison of biomass burning tracers during two haze episodes in the Daejeon
566 atmosphere

567 Levoglucosan and K^+ are widely used as indicators of biomass burning.

568 Levoglucosan is formed during pyrolysis of cellulose and hemicellulose, and is not

569 emitted from the burning of other materials, such as fossil fuels (Simoneit et al., 1999;

570 Caseiro et al., 2009; Elias et al., 2001). However, caution is required when using K^+ as a

571 biomass-burning tracer because K^+ can also be emitted from sea salt and soil (Pio et al.,

572 2008). The mass concentration of biomass burning tracers and their ratios during the

573 Siberian forest fire and Chinese haze episodes are summarized in Tables 2 and 3.

574 Significantly elevated concentrations of levoglucosan were observed during the

575 Siberian forest fire episode, compared with smaller increases observed during the

576 Chinese haze episode (Fig. 9). Concentrations of levoglucosan during the Siberian

577 forest fire episode were measured to be $119.6 \pm 6.0 \text{ ng m}^{-3}$, approximately 6 times

578 higher than those during the Chinese haze episode ($22.3 \pm 11.8 \text{ ng m}^{-3}$), as listed in

579 Table 2. However, similar levels of K^+ were obtained during the Chinese haze ($0.27 \pm$

580 $0.08 \text{ } \mu\text{g m}^{-3}$) and Siberian forest fire ($0.33 \pm 0.07 \text{ } \mu\text{g m}^{-3}$) episodes. Thus, relatively

581 high levoglucosan/ K^+ ratios were observed during the Siberian forest fire episode (0.37

582 ± 0.06) compared with those (0.08 ± 0.03) observed during the Chinese haze episode

583 (Table 3). However, the levoglucosan/mannosan ratios observed during the Siberian

584 forest fire episodes (3.43 ± 0.11) are similar to those observed during the Chinese haze

585 episodes (4.81 ± 0.41), as shown in Table 3.

586 OC concentrations increased as levoglucosan and K^+ concentrations increased

587 during the Siberian forest fire episode (Fig. 11a). Elevated OC/EC ratios were also
588 observed during the Siberian forest fire episode (7.18 ± 0.2). Simultaneous increases in
589 K^+ , OC (Fig. 11b), and levoglucosan concentrations (Fig. 11c) during the Siberian forest
590 fire episode suggest that the K^+ originated primarily from the smoke plume during the
591 Siberian forest fire episode.

592 OC and levoglucosan concentrations observed during the Chinese haze episode are
593 similar to those observed during the non-episode period, as shown in Fig. 11a. However,
594 small increases in K^+ concentration were observed during the Chinese haze episode, as
595 shown in Fig. 11b, resulting in relatively small levoglucosan/ K^+ ratios during the
596 Chinese haze episode (0.08 ± 0.03) compared with those during the Siberian forest fire
597 episode (0.37 ± 0.06). This difference in levoglucosan/ K^+ ratios can be explained as
598 follows. First, different types of biomass burning might have occurred during the
599 Chinese haze episode compared with the Siberian forest fire episode. It can be
600 postulated that biomass-burning emissions with relatively low OC/ K^+ and
601 levoglucosan/ K^+ ratios might have contributed to observations made on the Korean
602 Peninsula during the Chinese haze episode.

603 Second, K^+ measured during the Chinese haze episode may have originated from
604 sources other than biomass burning. Because OC is predominantly emitted from
605 biomass burning, biomass-burning particles have relatively high OC/EC ratios and are
606 generally well correlated with biomass burning tracers (Cao et al., 2008; Cheng et al.,
607 2008; Popovicheva et al., 2014). The lack of significant increases in OC/EC ratio ($2.4 \pm$
608 0.4), and OC and levoglucosan concentrations during the Chinese haze episode
609 compared with non-episode measurements suggests that the elevated K^+ concentrations
610 observed during the Chinese haze episode might be due to emissions from other sources,

611 such as soil, sea salt, or industrial complexes. Chow et al. (2008) reported that 3.9%–
612 12.5% of $\text{PM}_{2.5}$ consisted of K^+ in stack samples from cement kiln manufacturing
613 processes. Positive correlations of K^+ with SO_4^{2-} and EC concentrations during the
614 Chinese haze episode (Fig. 9) also suggest that there were additional emissions of K^+
615 from anthropogenic sources other than biomass burning.

616 Elevated concentrations of levoglucosan and OC, and relatively high OC/EC ratios
617 (7.18 ± 0.2) suggest that the haze episode that occurred during late July 2014 was
618 caused primarily by the long-range transport of smoke emitted from Siberian forest fires.
619 However, significantly elevated SO_4^{2-} concentrations with relatively weak increases in
620 OC and levoglucosan concentrations and lower OC/EC ratios indicate that the Chinese
621 haze episode was caused primarily by anthropogenic pollutants emitted from industrial
622 complexes and urban cities in East China, with relatively little contribution from
623 biomass burning.

624

625 3.3.3 Tracking major sources of biomass burning during the Siberian forest fire episode

626 Levoglucosan/mannosan (Levo/Man) ratios and levoglucosan/ K^+ (Levo/ K^+) ratios
627 observed during the Siberian forest fire episode are compared with those from previous
628 chamber experiments and field studies in Fig. 12. Hardwood burning produces higher
629 Levo/Man ratios with a mean value of 26 (range: 2.2–195) (Fine et al., 2001, 2002,
630 2004a, 2004b; Schauer et al., 2001; Engling et al., 2006; Schmidl et al., 2008a; Bari et
631 al., 2009; Gonçalves et al., 2010), whereas softwood burning has lower Levo/Man ratios
632 (mean: 4.3, range: 2.5–6.7) (Fine et al., 2001, 2002, 2004a, 2004b; Schauer et al., 2001;
633 Hays et al., 2002; Engling et al., 2006; Inuma et al., 2007; Schmidl et al., 2008a;
634 Gonçalves et al., 2010). Grass (mean: 18, range: 9.2–39) and crop residue burnings

635 (mean: 29, range: 12–55) have relatively high Levo/Man ratios compared with leaf
636 burning (mean: 5.6, range: 5.1–6.0) (Sheesley et al., 2003; Engling et al., 2006, 2009;
637 Sullivan et al., 2008; Schmidl et al., 2008b; Oanh et al., 2011; Cheng et al., 2013).
638 Levo/Man ratios (mean: 5.3) observed during the smoke episode in Moscow, Russia in
639 summer 2010 are similar to those reported for softwood and leaf burning (Popovicheva
640 et al., 2014).

641 Because levoglucosan and mannosan are emitted from similar burning processes,
642 the Levo/Man ratio can be used to track the type of biomass burning. Levo/Man ratios
643 observed during the Siberian forest fire episode are similar to those obtained from the
644 softwood and leaf burning experiments, and the smoke episode in Moscow, Russia
645 during summer 2010. However, Levo/Man ratios during the Siberian forest fire episode
646 are much lower than those reported for hardwood, grass, and crop residue burning.

647 Hardwood and softwood burning yields relatively high Levo/K⁺ ratios, with mean
648 values of 26 and 46, and ranges of 2.2–195 and 4.6–261, respectively (Fine et al., 2001,
649 2002, 2004a, 2004b; Schauer et al., 2001; Hays et al., 2002; Engling et al., 2006; Iinuma
650 et al., 2007; Schmidl et al., 2008a; Bari et al., 2009; Gonçalves et al., 2010). However,
651 grass, crop residue, and leaf burning have relatively low Levo/K⁺ ratios, with mean
652 values of 3.3, 0.53, and 2.9, and ranges of 0.06–9.5, 0.1–1.2, and 2.4–3.4, respectively
653 (Sheesley et al., 2003; Engling et al., 2006, 2009; Sullivan et al., 2008; Schmidl et al.,
654 2008b; Oanh et al., 2011; Cheng et al., 2013). Levo/K⁺ ratios (mean: 2.8) observed
655 during the smoke episode in Moscow, Russia in summer 2010 are similar those reported
656 for grass, crop residue, and leaf burning (Popovicheva et al., 2014).

657 Levo/K⁺ ratios observed during the Siberian forest fire episode are close to those
658 reported for grass, crop residue, and leaf burning, as well as to the ratios of the smoke

659 episode in Moscow, but much lower than those from hardwood and softwood burning
660 (Fig. 12b). Levoglucosan can be removed through photo-oxidative decay during
661 atmospheric transport (Hennigan et al., 2010), but K^+ is relatively stable in the
662 atmosphere. Thus, Levo/ K^+ ratios can decrease during long-range atmospheric transport.
663 The Levo/ K^+ ratios observed during the Siberian forest fire episode were lower than
664 those during the smoke episode in Moscow, Russia in summer 2010, which can be
665 explained by photochemical degradation of levoglucosan during long-range atmospheric
666 transport.

667 Based on a comparison of biomass burning tracers from various sources (Fig. 12), it
668 is suggested that smoke aerosol emitted during the Siberian forest fire episode
669 originated mainly from the burning of forest leaves in Siberia prior to their long-range
670 atmospheric transport. Smoke aerosol observed during the smoke episode in Moscow,
671 Russia in summer 2010 have similar Levo/Man and Levo/ K^+ ratios to those from leaf
672 burning (Fig. 12). These observations suggest that smoke episodes in the Russian forest
673 originate primarily from the burning of forest leaves.

674

675 4. Conclusion

676 This study investigated the long-range transport of smoke plumes emitted from
677 Siberian forest fires during late July 2014. Smoke plumes emitted from Siberian forest
678 fires are generally transported to the Northwest Pacific by prevailing westerlies.
679 However, the haze plume that occurred during late July 2014 had a significant impact
680 on the Korean Peninsula, which is located ~3000 km south of the Siberian forest. From
681 the spatial distributions of AOD obtained from the MODIS satellite, CALIPSO satellite
682 observations, and HYSPLIT air mass backward trajectory analyses, it is evident that

683 smoke plumes originating from Siberian forest fires between 23 and 24 July 2014 were
684 transported over 3000 km south to the Korean Peninsula between 27 and 28 July 2014.
685 During this episode, elevated concentrations of levoglucosan ($119.6 \pm 6.0 \text{ ng m}^{-3}$) and
686 K^+ ($0.33 \pm 0.07 \text{ } \mu\text{g m}^{-3}$), and high OC/EC ratios (7.18 ± 0.2) were observed at a
687 measurement site in Daejeon, Korea. These results suggest that the haze episode that
688 occurred during late July 2014 was caused mainly by the long-range transport of smoke
689 plumes emitted from Siberian forest fires. The Siberian smoke episode is clearly
690 distinguished from a haze episode caused by the long-range transport of anthropogenic
691 pollutants emitted from East China, which was characterized by elevated SO_4^{2-}
692 concentrations and weak increases in OC and levoglucosan concentrations.

693

694 Acknowledgements

695 This work was conducted as part of a co-research project between National Institute of
696 Environmental Research (NIER) and the Korean Research Institute of Standards and
697 Science (KRISS). This work was funded by the National Research Foundation under
698 grant NRF-2015R1C1A1A02036580. We thank Dr. B. Holben and Dr. M. Panchenko
699 for their efforts in establishing and maintaining the Yakutsk and Ussuriysk AERONET
700 sites in Russia. The authors gratefully acknowledge the NOAA Air Resources
701 Laboratory (ARL) for the provision of the HYSPLIT transport and dispersion model
702 and the READY website (<http://www.arl.noaa.gov/ready.html>) used in this publication.
703 The authors also thank NASA (USA) for making available the Collection 005 Level-2
704 MODIS data.

705

706

707 **Reference**

708

709 Bartalev, S. A., Korovin, G. N., and Shlepak, B. V.: Assessments of Forest Fire
710 Recognition, Using the NOAA AVHRR Radiometers, in: Proceedings of
711 International Forum on Problems in Science, Technology and Education, Vol. II,
712 Moscow, 22–25, 1977.

713 Bari, M. A., Baumbach, G., Kuch, B., and Scheffknecht, G.: Wood smoke as a source of
714 particle-phase organic compounds in residential areas, *Atmos. Environ.*, 43, 4722–
715 4732, 2009.

716 Birch, M. E., and Cary, R. A.: Elemental carbon-based method for monitoring
717 occupational exposure to particulate diesel exhaust, *Aerosol Sci. Tech.*, 25, 221–
718 241, 1996.

719 Bondur, V. G.: Importance of aerospace remote sensing approach to the monitoring of
720 nature fire in Russia, *International Forest Fire News (IFFN)*, (40), 43–57, 2010.

721 Cao, G., Zhang, X., Gong, S., and Zheng, F.: Investigation on emission factors of
722 particulate matter and gaseous pollutants from crop residue burning, *J. Environ.*
723 *Sci.*, 20, 50–55, 2008.

724 Carvalho, A., Monteiro, A., Flannigan, M., Solman, S., Miranda, A. I., and Borrego, C.:
725 Forest fires in a changing climate and their impacts on air quality, *Atmos. Environ.*,
726 45, 5545–5553, 2011.

727 Caseiro, A., Bauer, H., Schmidl, C., Pio, C. A., and Puxbaum, H.: Wood burning impact
728 on PM₁₀ in three Austrian regions, *Atmospheric Environment*, 43, 2186–2195, 2009.

729 Chan, C. K., and Yao, X.: Air pollution in mega cities in China, *Atmos. Environ.*, 42, 1–
730 42, 2008.

731 Cheng, M. T., Horng, C. L., Su, Y. R., Lin, L. K., Lin, Y. C., and Chou, C. K.:
732 Particulate matter characteristics during agricultural waste burning in Taichung City,
733 Taiwan, *J. Hazard. Mater.*, 165, 187–192, 2008.

734 Cheng, Y., Engling, G., He, K. B., Duan, F. K., Ma, Y. L., Du, Z. Y., Liu, J. M., Zheng,
735 M., and Weber, R. J.: Biomass burning contribution to Beijing aerosol, *Atmos.*
736 *Chem. Phys.*, 13, 7765–7781, 2013.

737 Chow, J. C., Watson, J. G., Kuhns, H., Etyemezian, V., Lowenthal, D. H., Crow, D.,

738 Kohl, S. D., Engelbrecht, J. P., and Green, M. C.: Source profiles for industrial,
739 mobile, and area sources in the Big Bend Regional Aerosol Visibility and
740 Observational study, *Chemosphere*, 54, 185–208, 2004.

741 Conard, S. G., and Ivanova, G. A.: A Differential Approach to Numerical Assessment of
742 Forest Fire Carbon Emissions, *Lesovedenie (Forestry)*, 3, 28–35, 1988.

743 Crutzen, P., Heidt, L., Krasnec, J., Pollock, W., and Seiler, W.: Biomass burning as a
744 source of atmospheric gases CO, H₂, N₂O, NO, CH₃Cl and COS, *Nature*, 282
745 (5736), 253–256, 1979.

746 Du, H., Kong, L., Cheng, T., Chen, J., Du, J., Li, L., Xia, X., Leng, C., and Huang, G.:
747 Insights into summertime haze pollution events over Shanghai based on online
748 water-soluble ionic composition of aerosols, *Atmos. Environ.*, 45, 5131–5137, 2011.

749 Elias, V. O., Simoneit, B. R. T., Cordeiro, R. C., and Turcq, B.: Evaluating levoglucosan
750 as an indicator of biomass burning in Carajás, Amazônia: a comparison to the
751 charcoal record, *Geochim. Cosmochim. Acta*, 65, 267–272, 2001.

752 Engling, G., Carrico, C.M., Kreidenweis, S. M., Collett Jr, J. L., Day, D. E., Malm, W.
753 C., Lincoln, L., Hao, W. M., Iinuma, Y., and Herrmann, H.: Determination of
754 levoglucosan in biomass combustion aerosol by high-performance anion-exchange
755 chromatography with pulsed amperometric detection, *Atmos. Environ.*, 40, S299–
756 S311, 2006.

757 Engling, G., Lee, J. J., Tsai, Y. W., Lung, S. C. C., Chou, C. C. K., and Chan, C. Y.:
758 Size-resolved anhydrosugar composition in smoke aerosol from controlled field
759 burning of rice straw, *Aerosol Sci. Tech.*, 43, 662–672, 2009.

760 Fine, P. M., Cass, G. R., and Simoneit, B. R. T.: Chemical characterization of fine
761 particle emissions from fireplace combustion of woods grown in the northeastern
762 United States, *Environ. Sci. Tech.*, 35, 2665–2675, 2001.

763 Fine, P. M., Cass, G. R., and Simoneit, B. R. T.: Chemical characterization of fine
764 particle emissions from the fireplace combustion of woods grown in the southern
765 United States, *Environ. Sci. Tech.*, 36, 1442–1451, 2002.

766 Fine, P. M., Cass, G. R., and Simoneit, B. R. T.: Chemical characterization of fine
767 particle emissions from the fireplace combustion of wood types grown in the
768 midwestern and western United States, *Environ. Eng. Sci.*, 21, 387–409, 2004a.

769 Fine, P. M., Cass G. R., and Simoneit, B. R. T.: Chemical characterization of fine

770 particle emissions from the wood stove combustion of prevalent United States tree
771 species, *Environ. Eng. Sci.*, 21, 705–721, 2004b.

772 Gonçalves, C., Alves, C., Evtugina, M., Mirante, F., Pio, C., Caseiro, A., Schmidl, C.,
773 Bauer, H., and Carvalho, F.: Characterisation of PM₁₀ emissions from wood stove
774 combustion of common woods grown in Portugal, *Atmos. Environ.*, 44, 4474–4480,
775 2010.

776 Hays, M. D., Geron, C. D., Linna, K. J., Smith, N. D., and Schauer, J. J.: Speciation of
777 gas-phase and fine particle emissions from burning of foliar fuels, *Environ. Sci.*
778 *Tech.*, 36, 2281–2295, 2002.

779 Hennigan, C. J., Sullivan, A. P., Collett Jr, J. L., and Robinson, A. L.: Levoglucosan
780 stability in biomass burning particles exposed to hydroxyl radicals, *Geophys. Res.*
781 *Lett.*, 37, doi:10.1029/2010GL043088, 2010.

782 Huang, X. F., He, L., Hu, M., Canganatna, M. R., Kroll, J. H., Ng, N. L., Zhang, Y. H.,
783 Lin, Y., Xue, L., Sun, T. L., Liu, X. G., Shao, M., Jayne, J. T., and Worsnop, D. R.:
784 Characterization of submicron aerosols at a rural site in Pearl River Delta of China
785 using an Aerodyne High-Resolution Aerosol Mass Spectrometer, *Atmos. Chem.*
786 *Phys.*, 11, 1865–1877, 2011.

787 Iinuma, Y., Brüggemann, E., Gnauk, T., Müller, K., Andreae, M. O., Helas, G., Parmar,
788 R., and Herrmann, H.: Source characterization of biomass burning particles: The
789 combustion of selected European conifers, African hardwood, savanna grass, and
790 German and Indonesian peat, *J. Geophys. Res.*, 112, D08209,
791 doi:10.1029/2006JD007120, 2007.

792 Isaev, A. S., Korovin, G. N., Bartalev, S. A., Ershov, D. V., Janetos, A., Kasischke, E. S.,
793 Shugart, H. H., French, N. H. F., Orlick, B. E., and Murphy, T. L.: Using Remote
794 Sensing to Assess Russian Forest Fire Carbon Emissions, *Climatic Change*, 55,
795 235–249, 2002.

796 Jeong, H., Chung, C. E., van Noije, T., and Takemura, T.: Relationship between fine-
797 mode AOD and precipitation on seasonal and interannual time scales, *Tellus Ser. B*,
798 66, 23037, doi:10.3402/tellusb.v66.23037, 2014.

799 Jeong, J. I., Park, R. J., and Youn, D.: Effects of Siberian forest fires on air quality in
800 East Asia during May 2003 and its climate implication, *Atmos. Environ.*, 42, 8910–
801 8922. doi:10.1016/j.atmosenv.2008.08.037, 2008.

- 802 Kajii, Y., Kato, S., Streets, D. G., Tsai, N. Y., Shvidenko, A., Nilsson, S., Minko, N. P.,
803 Abushenko, N., Altyntsev, D., and Khodzer, T. V.: Boreal forest fires in Siberia in
804 1998: estimation of area and emissions of pollutants by AVHRR satellite data, *J.*
805 *Geophys. Res.*, 107 (D24), 4745, 2002.
- 806 Kanaya, Y., Kajii, Y., and Akimoto, H.: Solar actinic flux and photolysis frequency
807 determinations by radiometers and a radiative transfer model at Rishiri Island:
808 comparisons, cloud effects, and detection of an aerosol plume from Russian forest
809 fires, *Atmos. Environ.*, 37 (18), 2463–2475, 2003.
- 810 Lee, K. H., Kim, J. E., Kim, Y. J., Kim, J., and Von Hoyningen-Huene, W.: Impact of
811 the smoke aerosol from Russian forest fires on the atmospheric environment over
812 Korea during May 2003, *Atmos. Environ.*, 39, 85–99, 2005.
- 813 Li, B., Zhang, J., Zhao, Y., Yuan, S., Zhao, Q., Shen, G., and Wu, H.: Seasonal variation
814 of urban carbonaceous aerosols in a typical city Nanjing in Yangtze River Delta,
815 *China, Atmos. Environ.*, 106, 223–231, 2015.
- 816 Li, L., An, J. Y., Zhou, M., Yan, R. S., Huang, C., Lu, Q., Lin, L., Wang, Y. J., Tao, S. K.,
817 Qiao, L. P., Zhu, S. H., and Chen, C. H.: Source apportionment of fine particles and
818 its chemical components over the Yangtze River Delta, China during a heavy haze
819 pollution episode, *Atmos. Environ.*,
820 <http://dx.doi.org/10.1016/j.atmosenv.2015.06.051>, 2015(in press).
- 821 Mei, L., Xue, Y., de Leeuw, G., Guang, J., Wang, Y., Li, Y., Xu, H., Yang, L., Hou, T.,
822 He, X., Wu, C., Dong, J., and Chen, Z.: Integration of remote sensing data and
823 surface observations to estimate the impact of the Russian wildfires over Europe
824 and Asia during August 2010, *Biogeosciences*, 8, 3771–3791, 2011.
- 825 Oanh, N. T. K., Ly, B. T., Tipayarom, D., Manandhar, B. R., Prapat, P., Simpson, C. D.,
826 and Liu, L. J. S.: Characterization of particulate matter emission from open burning
827 of rice straw, *Atmos. Environ.*, 45, 493–502, 2011.
- 828 Pio, C. A., Legrand, M., Alves, C. A., Oliveira, T., Afonso, J., Caseiro, A., Puxbaum, H.,
829 Sanchez-Ochoa, A., and Gelencsér, A.: Chemical composition of atmospheric
830 aerosols during the 2003 summer intense forest fire period, *Atmos. Environ.*, 42,
831 7530–7543, 2008.
- 832 Popovicheva, O., Kistler, M., Kireeva, E., Persiantseva, N., Timofeev, M., Kopeikin, V.,
833 and Kasper-Giebl, A.: Physicochemical characterization of smoke aerosol during

834 large-scale wildfires: Extreme event of August 2010 in Moscow, *Atmos. Environ.*,
835 96, 405–414, 2014.

836 Quennehen, B., Schwarzenboeck, A., Matsuki, A., Burkhart, J. F., Stohl, A., Ancellet, G.,
837 and Law, K. S.: Anthropogenic and forest fire pollution aerosol transported to the
838 Arctic: observations from the POLARCAT-France spring campaign, *Atmos. Chem.*
839 *Phys.*, 12, 6437–6454, 2012.

840 Schauer, J. J., Kleeman, M. J., Cass, G. R., and Simoneit, B. R. T.: Measurement of
841 emissions from air pollution sources. 3. C1-C29 organic compounds from fireplace
842 combustion of wood, *Environ. Sci. Tech.*, 35, 1716–1728, 2001.

843 Schmidl, C., Marr, I. L., Caseiro, A., Kotianová, P., Berner, A., Bauer, H., Kasper-Giebl,
844 A., and Puxbaum, H.: Chemical characterisation of fine particle emissions from
845 wood stove combustion of common woods growing in mid-European Alpine
846 regions, *Atmos. Environ.*, 42, 126–141, 2008a.

847 Schmidl, C., Bauer, H., Dattler, A., Hitzenberger, R., Weissenboeck, G., Marr, I. L., and
848 Puxbaum, H.: Chemical characterisation of particle emissions from burning leaves,
849 *Atmos. Environ.*, 42, 9070–9079, 2008b.

850 Schreier, S. F., Richter, A., Schepaschenko, D., Shvidenko, A., Hilboll, A., and Burrows,
851 J.P.: Differences in satellite-derived NO_x emission factors between Eurasian and
852 North American boreal forest fires, *Atmos. Environ.*, 121, 55–65, 2015.

853 Sheesley, R. J., Schauer, J. J., Chowdhury, Z., Cass, G. R., and Simoneit, B. R. T.:
854 Characterization of organic aerosols emitted from the combustion of biomass
855 indigenous to South Asia, *J. Geophys. Res.*, 108, 4285, doi:10.1029/2002JD002981,
856 2003.

857 Simoneit, B. R. T., Schauer, J. J., Nolte, C. G., Oros, D. R., Elias, V. O., Fraser, M. P.,
858 Rogge, W. F., and Cass, G. R.: Levoglucosan, a tracer for cellulose in biomass
859 burning and atmospheric particles, *Atmos. Environ.*, 33, 173–182, 1999.

860 Sullivan, A. P., Holden, A. S., Patterson, L. A., McMeeking, G. R., Kreidenweis, S. M.,
861 Malm, W. C., Hao, W. M., Wold, C. E., and Collett Jr., J. L.: A method for smoke
862 marker measurements and its potential application for determining the contribution
863 of biomass burning from wildfires and prescribed fires to ambient PM_{2.5} organic
864 carbon, *J. Geophys. Res.*, 113, D22302, doi:10.1029/2008JD010216, 2008.

865 Wu, R., Bo, Y., Li, J., Li, L., Li, Y., and Xie, S.: Method to establish the emission

866 inventory of anthropogenic volatile organic compounds in China and its application
867 in the period 2008-2012, *Atmos. Environ.*, 127, 244–254, 2016.
868 Youn, D., Park, R. J., Jeong, J. I., Moon, B. K., Yeh, S. W., Kim, Y. H., Woo, J. H., Im,
869 E. G., Jeong, J. H., Lee, S. J., and Song, C. K.: Impacts of aerosols on regional
870 meteorology due to Siberian forest fires in May 2003, *Atmos. Environ.*, 45, 1407–
871 1412, 2011.

Table 1. Measurement parameters and conditions of the present study.

Measurement parameters	Site	Sampling method	Measurement method	Data frequency
PM _{2.5} mass	Daejeon, Korea	Online measurement	Beta-attenuation monitor	1 h
Levogluconan, Mannosan	Daejeon, Korea	PM _{2.5} filter sampling	High-performance anion-exchange chromatography	1 day
Water-soluble ions (NO ₃ ⁻ , SO ₄ ²⁻ , etc)	Daejeon, Korea	PM _{2.5} filter sampling	Ion chromatography	1 day
Organic carbon (OC), elemental carbon (EC)	Daejeon, Korea	Online measurement	Semi-continuous OC/EC analyzer	1 h
Aerosol optical depth (AOD)	Yakutsk and Ussuriysk, Russia	Online measurement	Sunphotometer	~15 min

Table 2. Summary of fine particle (PM_{2.5}) mass, and organic and inorganic chemical composition of PM_{2.5} particles during the Chinese haze and Siberian forest fire episodes measured at Daejeon, Korea during summer 2014.

Components	Unit	¹⁾ Chinese Haze	²⁾ Siberian Forest Fire
		Range (Average \pm 1 σ)	
PM _{2.5} mass		44.5–65.1 (52.3 \pm 11.1)	44.3–56.2 (50.2 \pm 8.4)
SO ₄ ²⁻		20.9–25.1 (23.1 \pm 2.1)	7.4–9.2 (8.3 \pm 1.3)
NO ₃ ⁻		0.9–5.0 (2.8 \pm 2.1)	1.1–1.7 (1.4 \pm 0.4)
NH ₄ ⁺	($\mu\text{g m}^{-3}$)	6.1–12.7 (10.0 \pm 3.5)	4.6–5.4 (5.0 \pm 0.6)
OC		3.6–5.7 (4.8 \pm 1.1)	10.0–11.6 (10.8 \pm 1.1)
EC		1.9–2.2 (2.0 \pm 0.2)	1.4–1.6 (1.5 \pm 0.2)
K ⁺		0.17–0.33 (0.27 \pm 0.08)	0.28–0.38 (0.33 \pm 0.07)
OC/EC ratio		1.93–2.64 (2.4 \pm 0.41)	7.04–7.32 (7.18 \pm 0.19)
Levogluconan		13.4–35.7 (22.3 \pm 11.8)	115.4–123.9 (119.6 \pm 6.0)
Mannosan	(ng m^{-3})	3.0–6.8 (4.5 \pm 2.0)	32.9–37.0 (34.9 \pm 2.9)

¹⁾Chinese haze: 14–16 July 2014

²⁾Siberian forest fire: 27–28 July 2014

Table 3. Summary of ratios of biomass burning tracers during the Chinese haze and Siberian forest fire episodes, as measured at Daejeon, Korea in summer 2014.

Components	Chinese Haze	Siberian Forest Fire
	Range (Average \pm 1 σ)	
Levoglucosan/Mannosan ratio	4.41–5.22 (4.81 \pm 0.41)	3.35–3.51 (3.43 \pm 0.11)
Levoglucosan/K ⁺ ratio	0.05–0.11 (0.08 \pm 0.03)	0.33–0.41 (0.37 \pm 0.06)

Figure captions

Fig. 1. Map of the measurement site (36.19°N, 127.24°E) in Daejeon, Korea (base map from Google Maps). The Siberian forest is located ~3000 km north of the Korean Peninsula.

Fig. 2. Temporal variations in the chemical components of fine particulate matter (PM_{2.5}) at the Daejeon site during July 2014.

Fig. 3. (a) MODIS RGB image on 25 July 2014 and (b) air mass backward trajectories between 26 and 28 July 2014 when smoke plumes originating from Siberian forest fires had an impact on the Korean Peninsula. Red, blue, and green in (b) represent air mass backward trajectories arriving at 200 m, 500 m, and 1000 m heights, respectively. The Yakutsk site (61.66°N, 129.37°E) and Ussuriysk site (43.70°N, 132.16°E) in (b) are AERONET sites in Russia.

Fig. 4. MODIS AOD over East Asia from 23 to 28 July 2014.

Fig. 5. Temporal variations in AOD measured by a sun-photometer at the Yakutsk and Ussuriysk sites in Russia during July 2014.

Fig. 6. MODIS RGB images and vertical profiles of total attenuated backscatter at 532 nm measured by the CALIPSO satellite during (a) 24, (b) 25, and (c) 27 July 2014. Yellow lines in the MODIS RGB images indicate the route of the CALIPSO satellite, and correspond to the x-axis in the vertical profiles of total attenuated backscatter.

Fig. 7. (a) MODIS RGB image on 14 July 2014 and (b) air mass backward trajectories between 15 and 16 July 2014 when haze plumes originating from East China had an impact on the Korean Peninsula.

Fig. 8. MODIS AOD over East Asia between 13 and 15 July 2014.

Fig. 9. Temporal variations in PM_{2.5} mass, K⁺, levoglucosan, OC, EC, and SO₄²⁻ concentrations at the Daejeon site over the entire measurement period.

Fig. 10. Average relative contributions to PM_{2.5} mass during the (a) Chinese haze and (b) Siberian forest fire episodes.

Fig. 11. Scatter plots of OC versus (a) levoglucosan and (b) K⁺, and levoglucosan versus (c) K⁺ and (d) mannosan between 4 and 31 July 2014. Filled black and red diamonds represent the Chinese haze and Siberian forest fire episodes, respectively. Open black circles represent the remaining sampling days in July 2014.

Fig. 12. (a) Levoglucosan to mannosan ratios and (b) levoglucosan to K⁺ ratios obtained from previous chamber studies, extreme smoke episodes in Moscow, Russia in summer 2010, and the Siberian forest fire episode. **Hardwoods:** Fine et al. (2001, 2002, 2004a, 2004b), Schauer et al. (2001), Engling et al. (2006), Schmidl et al. (2008a), Goncalves et al. (2010), Bari et al. (2009); **Softwoods:** Fine et al. (2001, 2002, 2004a, 2004b), Schauer et al. (2001), Engling et al. (2006), Hay et al. (2002), Schmidl et al. (2008a), Goncalves et al. (2010), Iinuma et al. (2007), Cheng et al. (2013); **Grass:** Sullivan et al. (2008); **Crop residue:** Sullivan et al., (2008), Oanh et al. (2011), Sheesley et al. (2003), Engling et al. (2009), Cheng et al. (2013); **Leaf:** Schmidl et al. (2008b); **Moscow smoke:** Popovicheva et al. (2014); **LRT Siberia FF:** This study.

Figure 1

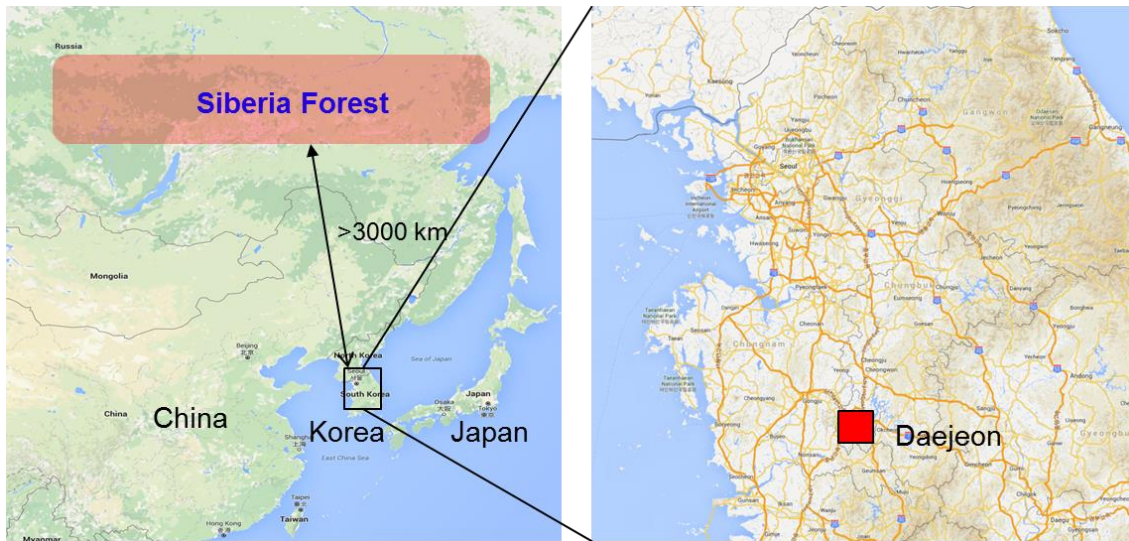


Figure 2

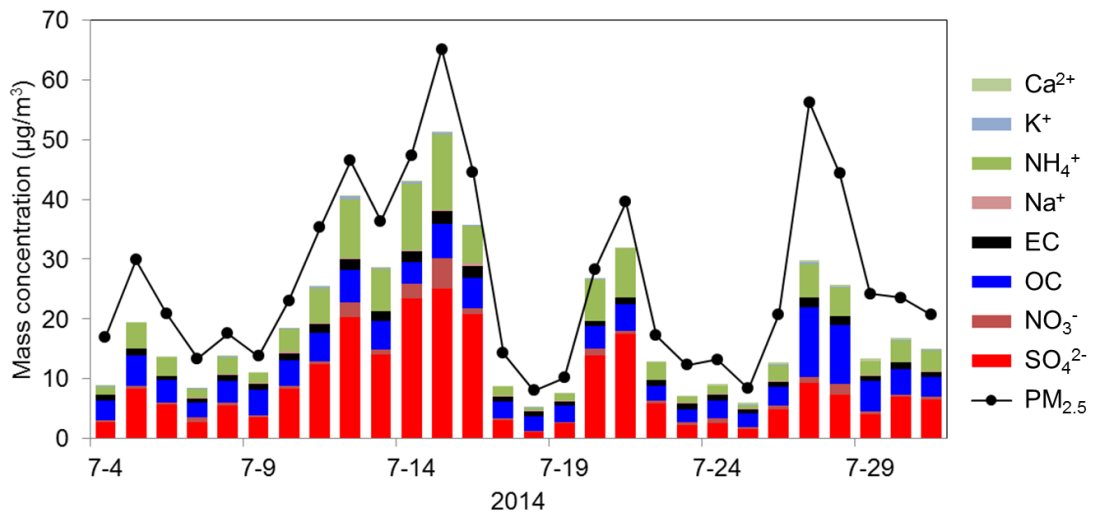
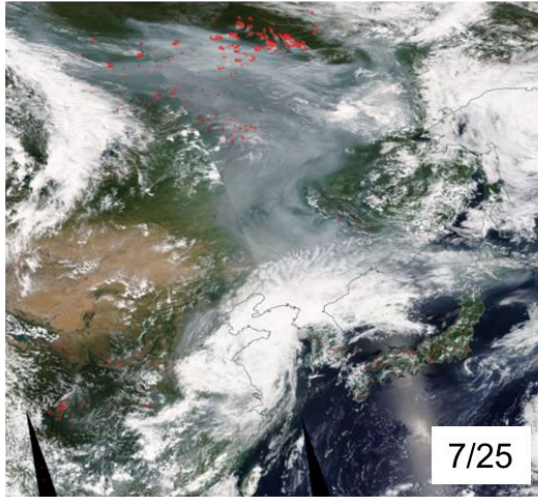


Figure 3

(a)



(b)



Figure 4

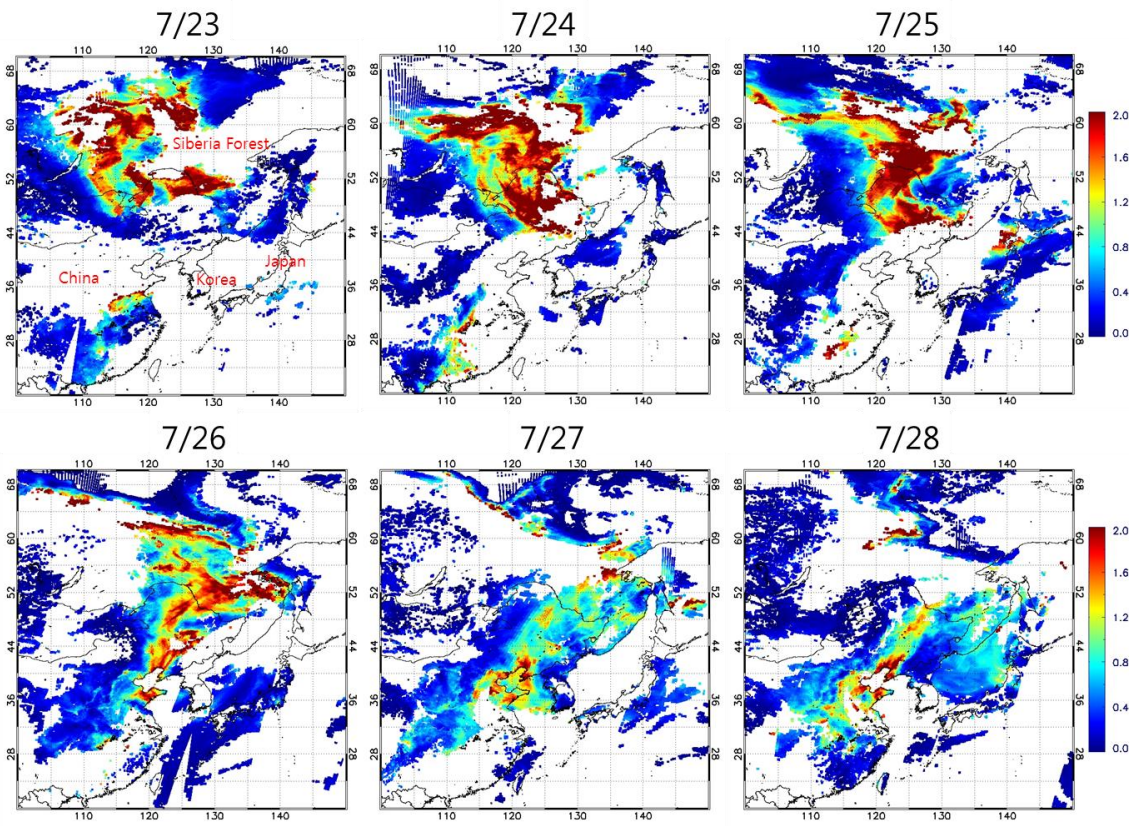


Figure 5

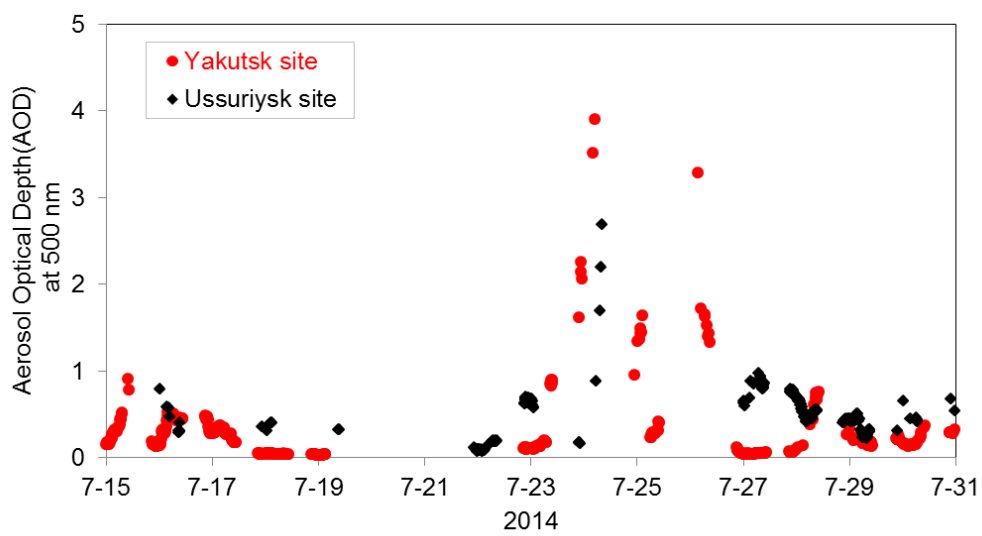


Figure 6

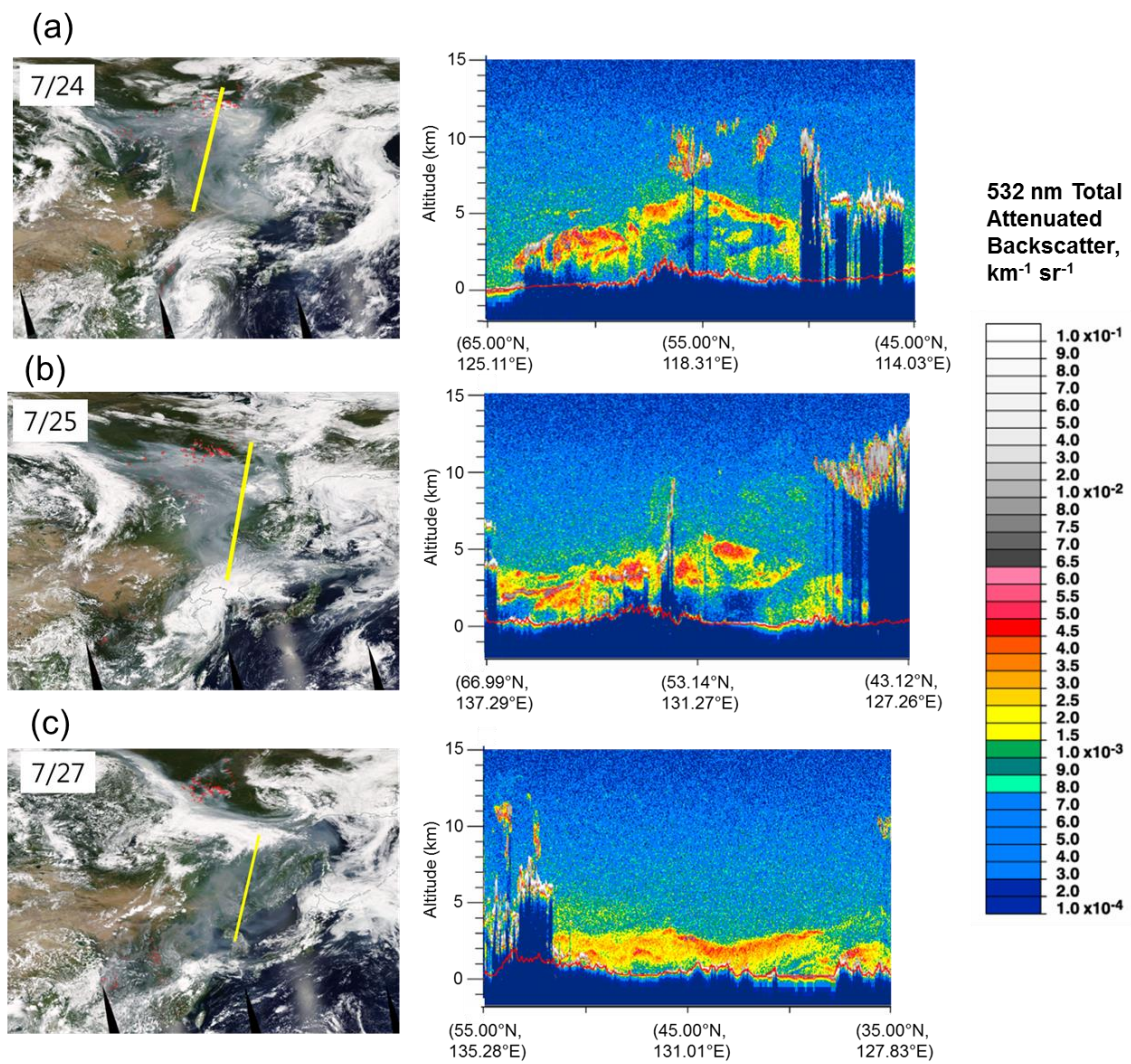
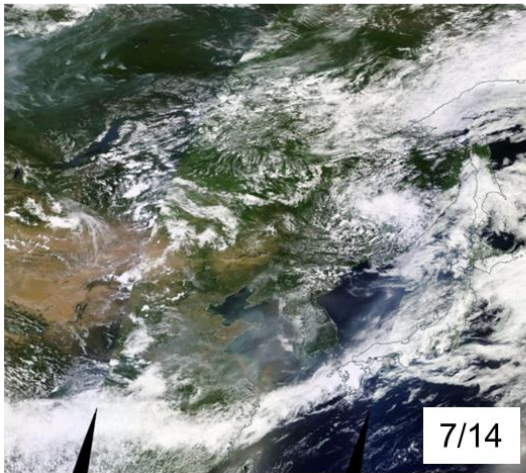


Figure 7

(a)



(b)

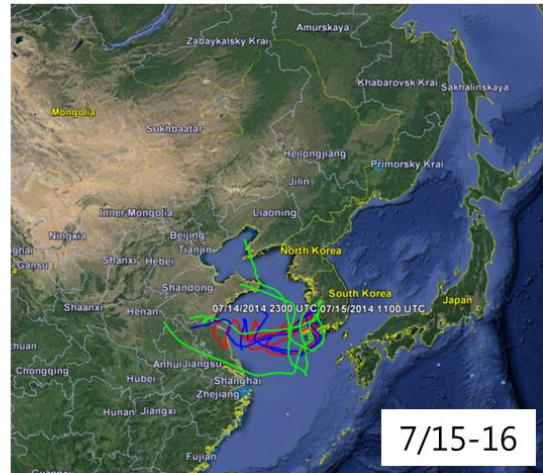


Figure 8

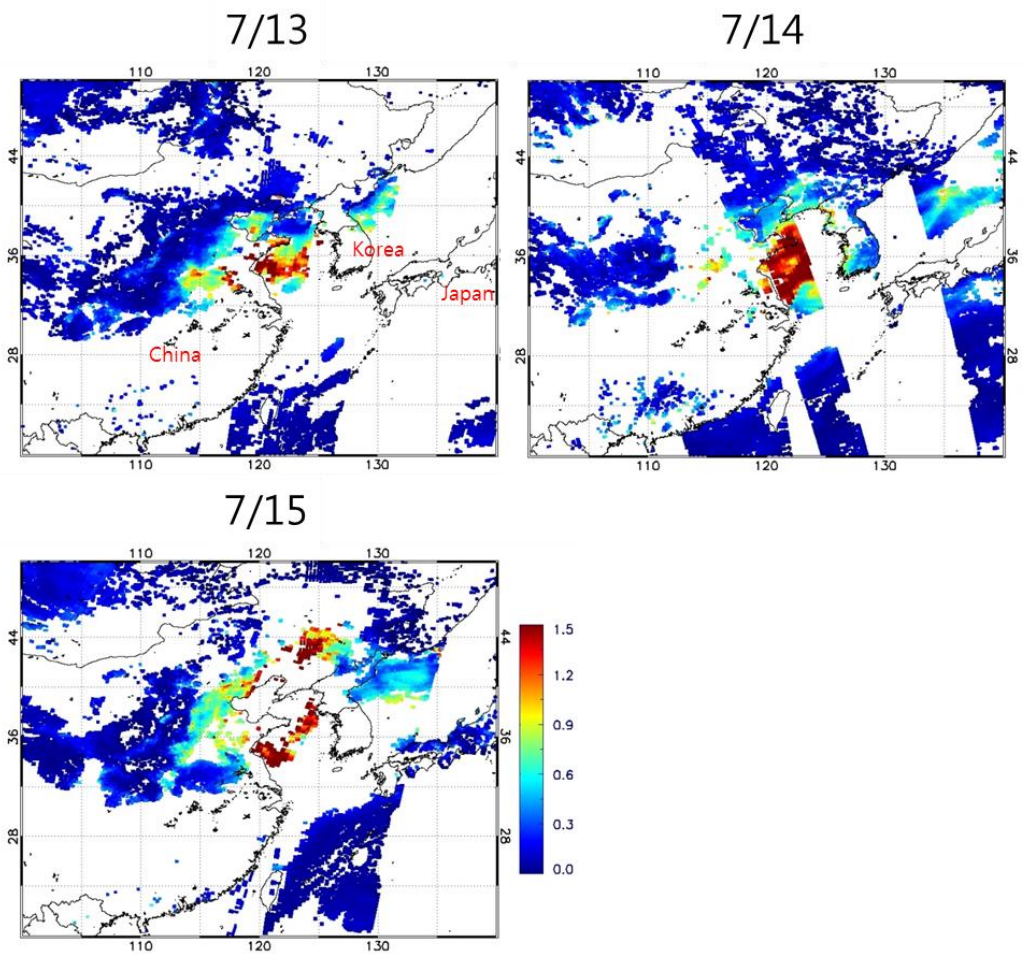


Figure 9

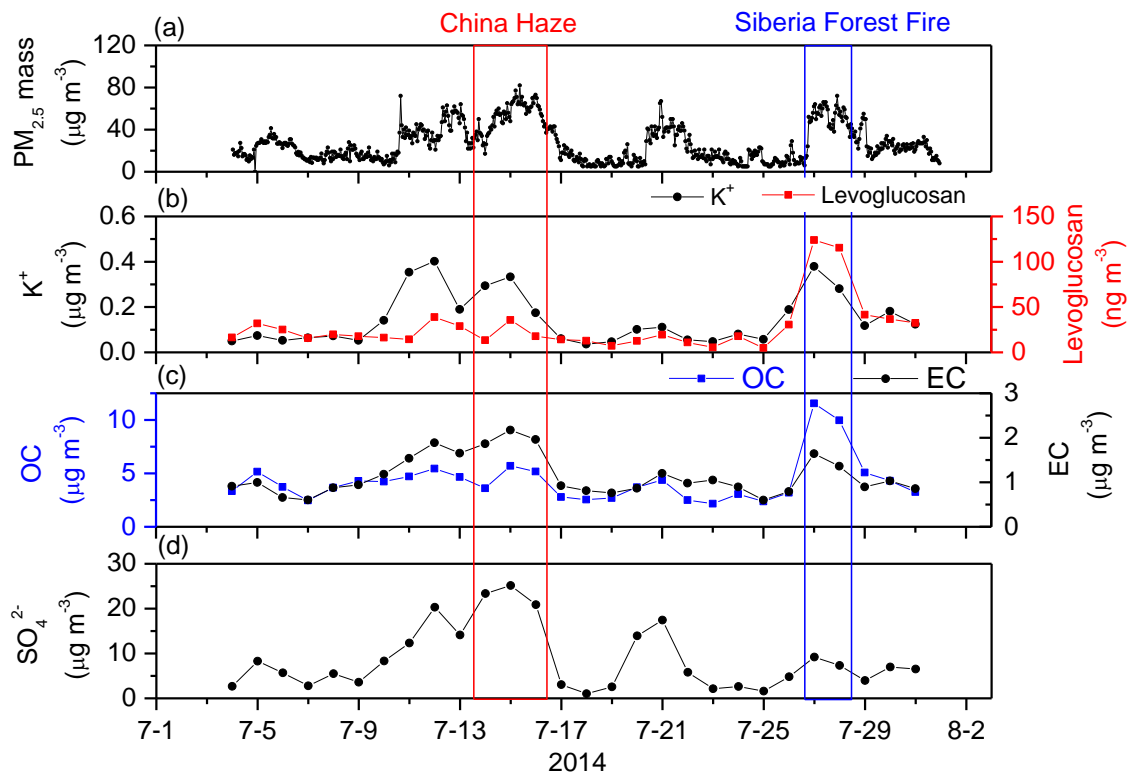


Figure 10

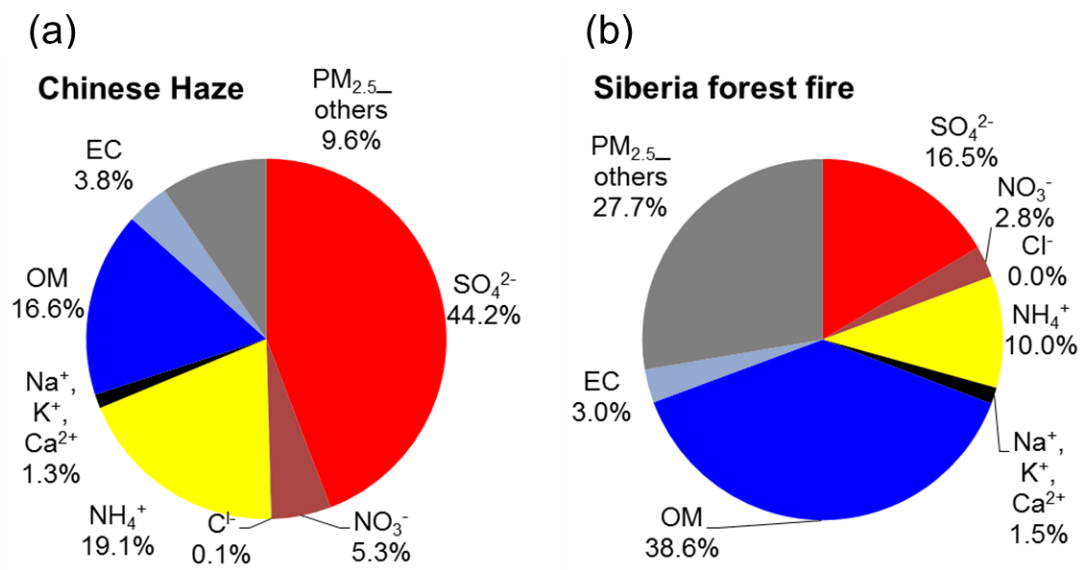


Figure 11

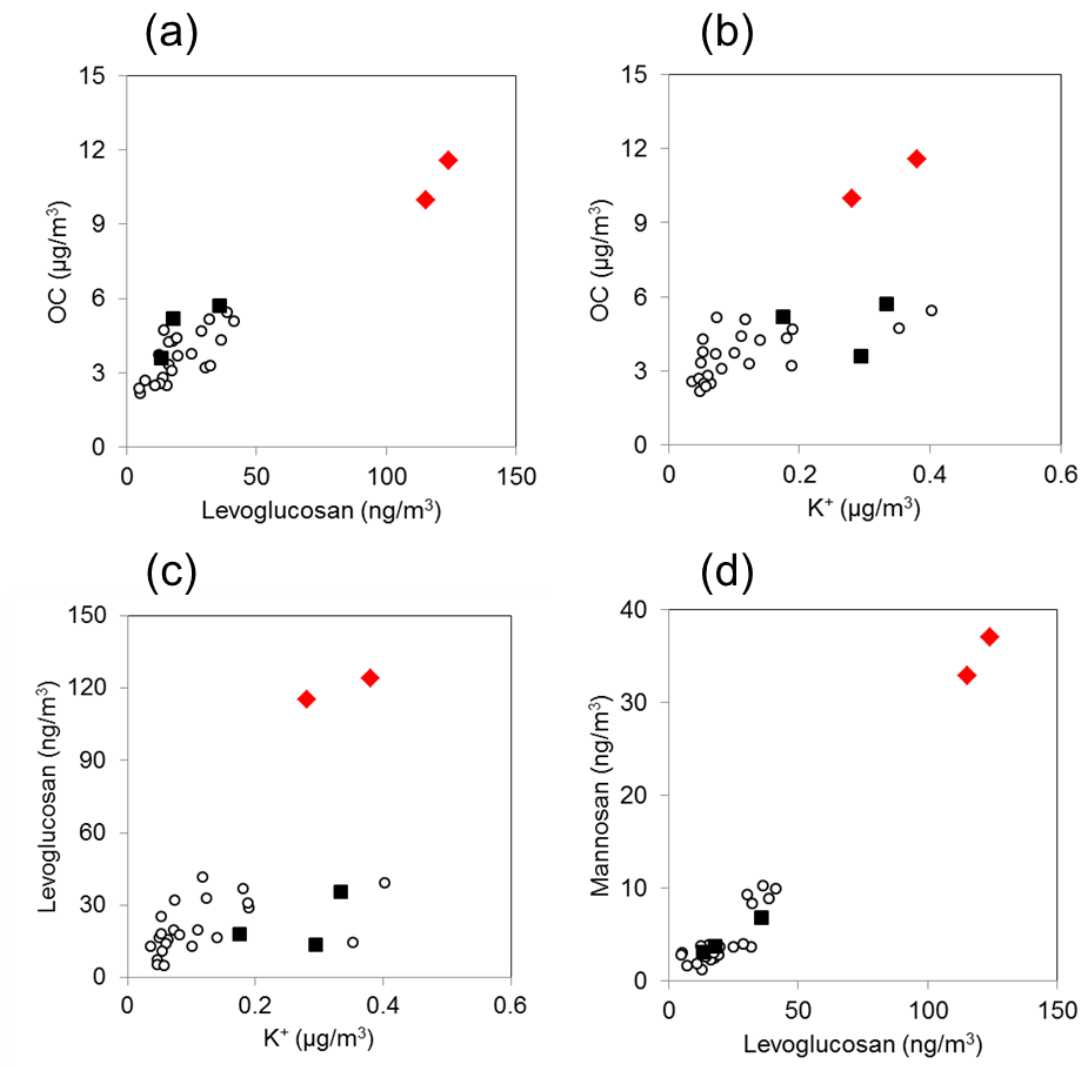


Figure 12

